PCCP

ROYAL SOCIETY OF CHEMISTRY

PERSPECTIVE

View Article Online
View Journal | View Issue

Cite this: *Phys. Chem. Chem. Phys.*, 2023, **25**, 19380

Green nanoparticle synthesis at scale: a perspective on overcoming the limits of pulsed laser ablation in liquids for high-throughput production

Inna Y. Khairani,[a] Gladys Mínguez-Vega,[b] Carlos Doñate-Buendía[a] and Bilal Gökce *[a]

Nanoparticles have become increasingly important for a variety of applications, including medical diagnosis and treatment, energy harvesting and storage, catalysis, and additive manufacturing. The development of nanoparticles with different compositions, sizes, and surface properties is essential to optimize their performance for specific applications. Pulsed laser ablation in liquid is a green chemistry approach that allows for the production of ligand-free nanoparticles with diverse shapes and phases. Despite these numerous advantages, the current production rate of this method remains limited, with typical rates in the milligram per hour range. To unlock the full potential of this technique for various applications, researchers have dedicated efforts to scaling up production rates to the gram-per-hour range. Achieving this goal necessitates a thorough understanding of the factors that limit pulsed laser ablation in liquid (PLAL) productivity, including laser, target, liquid, chamber, and scanner parameters. This perspective article explores these factors and provides a roadmap for increasing PLAL productivity that can be adapted to specific applications. By carefully controlling these parameters and developing new strategies for scaling up production, researchers can unlock the full potential of pulsed laser ablation in liquids.

Received 17th March 2023,
Accepted 19th May 2023

DOI: 10.1039/d3cp01214j

rsc.li/pccp

[a] *Chair of Materials Science and Additive Manufacturing, School of Mechanical Engineering and Safety Engineering, University of Wuppertal, 42119 Wuppertal, Germany. E-mail: goekce@uni-wuppertal.de*
[b] *GROC-UJI, Institut de Noves Tecnologies de la Imatge (INIT), Universitat Jaume I, 12071, Castellón, Spain*

Inna Y. Khairani

Inna Yusnila Khairani, MSc obtained her BSc summa cum laude from the Chemistry Department, Universitas Gadjah Mada, Indonesia. She was later awarded the Korean Government Scholarship Program (KGSP) at the Department of Materials Science and Engineering, Seoul National University (SNU) in South Korea, and graduated summa cum laude. During her master's degree, she won an award in a writing competition held by the SNU Foundation. She is currently a PhD candidate under the supervision of Prof. Bilal Gökce, and her task is to scale up the productivity of nickel–iron alloy nanoparticles produced by the pulsed laser ablation in liquid (PLAL).

Gladys Mínguez-Vega

Professor Gladys Mínguez Vega obtained her BSc and PhD degrees in Physics from the University of Valencia in 1997 and 2002, respectively. In 2002, she joined the Universitat Jaume I of Castellón (Spain). She has developed several research stays in the Centro de Investigaciones en Óptica (Mexico, 1998), the Applied Optics Institute (Poland, 2002), the Fernuniversität in Hagen (Germany, 2003), and the Purdue University (USA, 2004 and 2009). Her research interest includes ultrafast optics and the synthesis of nanomaterials with laser. Since 2017, she has co-led the Photonics research group "GROC·UJI," and in 2022, she became a Full Professor.

1. Introduction

Nanoparticles have been utilized by humans for centuries, with early examples dating back to the Roman Empire. The Lycurgus cup, a piece of Roman glassware from the 4th century AD, contains gold nanoparticles that provide a striking optical dichroism effect. The cup appears green when lit from the front but red when illuminated from the back, due to the interaction of light with the gold nanoparticles. This ancient artifact provides a remarkable testament to the unique properties of nanoparticles and their potential applications.[1,2] Since then, the field of nanotechnology has undergone tremendous growth. Nanoparticles, with sizes typically ranging from 1 to 100 nanometers, exhibit unique electronic, optical, and mechanical properties that differ from their bulk counterparts. Applications of NPs stretch from drug delivery and contrast agents for magnetic resonance in the biomedical field,[3–6] catalysts for the development of renewable energy systems and environment remediation,[7–10] for the photo- and electrocatalytic application,[11] such as the water-splitting process,[12] fabrication of solar nanofluids,[13] properties enhancement and smart materials printing by additive manufacturing,[14,15] to the development of food packaging with antibacterial effects in the food industry.[16–18] The broad application spectrum that nanotechnology has reached during the last decades has been possible due to the unique physicochemical properties of the NP compared to bulk materials. The increased surface area-to-volume ratio, which exposes more active sites, is key to enhancing catalysts' response. The possibility of tuning the optical, thermal, and conductivity properties depending on the particle size, surface functionalization, and doping has given rise to the sensors' development,[19–21] advanced materials,[22] and optoelectronic devices.[20,23,24]

The dependence of the NPs' properties on their physicochemical parameters represents a key advantage in many applications. However, in the previous century, the synthesis of NPs with controlled characteristics represented a major challenge, limiting application development. Even nowadays, with the appearance of novel materials and the continuous innovation of the current nanomaterials' functionalities, synthesis techniques represent a central pillar of nanotechnology development, requiring green methods that offer material versatility, size control, NP purity, controlled surface doping, and in many cases, high productivity to address the industrial demands.[25]

Nanoparticle synthesis techniques can be divided into two groups, top-down and bottom-up approaches. The top-down methods are based on the breaking of bulk material to achieve nanometer-sized particles, including methods such as ball-milling, sputtering, and thermal evaporation. Meanwhile, the bottom-up approaches involve building NPs through the joint of their atomic constituents, usually performed by chemical synthesis methods, such as co-precipitation, sol–gel, hydrothermal, and chemical vapor deposition methods. Laser ablation is typically considered a top-down approach to the synthesis of nanoparticles since it involves the use of laser energy to ablate bulk materials and create nanoparticles. Nevertheless, this method can also be considered a bottom-up approach due to the subsequent NPs formation through nucleation and growth processes of the material constituents generated by the high-intensity pulsed laser interaction.

Laser ablation can be performed within a vacuum, gas, or liquid medium.[11] The production of nanomaterials by laser ablation in a vacuum is mostly known as pulsed laser deposition (PLD), where the ablated nanomaterials are deposited onto a substrate after ablation.[26] This technique offers the versatility to produce thin films with controlled elemental composition by combining the ablation of different targets.[26] Besides, the film thickness can be controlled within the nano- to micrometer range.[27] Laser ablation can also be performed in a gas environment, either with a certain gas flow or in the air. In this case, the method is usually aimed to modify the target material to

Carlos Doñate-Buendía

Dr Carlos Doñate Buendía obtained his PhD in 2019 distinguished with the international mention and summa cum laude from the University Jaume I after being awarded a FPI-UJI contract to develop nanomaterials by high throughput pulsed-laser based systems and their application in biomedicine and material processing. In 2020, he became postdoctoral researcher at the University of Duisburg-Essen working in the development of nanofunctionalized materials for additive manufacturing. In 2021, he joined the Chair of Materials Science and Additive Manufacturing at University of Wuppertal, where he is currently the group leader of the Particles and Additive Manufacturing of Polymers group.

Bilal Gökce

Professor Bilal Gökce completed his physics diploma at RWTH Aachen University in 2008 and his PhD in physics at North Carolina State University in 2012. After post-doctoral work on non-linear optics and a year at T-systems international, he joined the University of Duisburg-Essen in 2014 as a group leader for Laser Material Processing & Nanoparticle Generation. He achieved habilitation in 2018 and won the Fojtik-Henglein Prize. In 2020, he became a full professor at the University of Wuppertal, creating the Chair of Materials Science and Additive Manufacturing, after receiving the DFG Heisenberg Programme fellowship and being awarded with the Berthold-Leibinger-Innovation-Prize.

achieve the desired structure and properties, since the NPs will be re-deposited onto the surface of the target at a very fast rate.[28]

The production of nanomaterials using a laser in liquid is usually named laser ablation in liquid (LAL). It is based on the irradiation with a high-intensity laser beam ($>10^9$ W cm^{-2}) of a bulk target immersed in a liquid.[29] In LAL, two situations are generally differentiated depending on the laser source employed. When a continuous laser is employed, the technique is known as continuous wave laser ablation in liquid (CLAL), while the methodology is known as pulsed laser ablation in liquids (PLAL) if the source is a pulsed laser. Generally, the research field has evolved towards the standard employment of pulsed lasers, as the constant emission of light from the continuous wave laser heats the target and induces the boiling of the surrounding liquid. The boiling liquid scatters the incoming laser beam to the target, making CLAL unfeasible for continuous or large-scale NP production.

PLAL was first introduced in 1987 by Patil *et al.*[30] through the ablation of iron foils in water using a nanosecond laser and in 1993 by Fojtik and Henglein[31,32] for their work on laser synthesized-colloidal nanoparticles dispersed in a liquid. The operational steps of PLAL are relatively straightforward; the laser is directly shot onto a target fixed inside a liquid medium (Fig. 1). The ablated material is collected in the surrounding liquid media, avoiding user inhalation and safety risks, and directly producing colloidal nanoparticles of the desired material in the selected solvent. This technique gained popularity due to the possibility of producing bare-surface – ligand-free NPs, which offer improved catalytic activity, efficient conjugation, and higher affinity to biomolecules.[33–35] Furthermore, it is also possible to produce complex structures through PLAL, such as hollow NPs[36,37] and core–shell NPs,[38,39] which might require multiple steps in other synthesis methods.[40,41] Moreover, PLAL complies with green chemistry principles.[42] Most synthesis techniques require surfactants, certain solvents, gas atmospheres, and pre-and post-processing, such as stirring, heating, centrifugation, filtration, and annealing, to produce NPs.[43–45] Meanwhile, PLAL is usually performed in an ambient atmosphere, pressure, and temperature conditions, without the use of surfactants and hazardous substances, and with no or limited side products or waste generation.[46] Nevertheless, one critical drawback of this method is the low nanoparticle production rate. With the increase in the global population and its demands, the need for a more efficient way to synthesize PLAL nanomaterials will grow. Production rates achievable for oxide nanoparticles through the standard PLAL processes using an oxide target, typically on the order of milligrams per hour,[47–49] may be adequate for certain nanoparticle applications in bioimaging, biomedicine, and sensing, where only small amounts of nanoparticles are needed. However, increasing productivity to the grams per hour scale for the variety of nanomaterials produced by PLAL will reduce the synthesis cost, and possibly lower the market price and increase the interest of the NPs produced by this method.[50] As an example of PLAL productivity compared to high-yield chemical methods, the thermolysis of a metal oleate precursor has achieved a yield value of 40 grams of iron oxide NPs per batch.[51] Meanwhile, PLAL produces NPs in a scale of tens to hundreds of milligrams, which has been extended achieving g h^{-1} productivities for other metallic[52] and ceramic NPs,[53] and with a record of 8 grams per hour for Pt NPs produced by Waag *et al.*[54] in 2021.

The aim of this perspective article is to critically review the current status of PLAL productivity and provide strategies to continue upscaling the process. To understand the factors that limit PLAL productivity and provide a clear roadmap to overcome them, first, the PLAL technique principles will be described. Besides, to avoid ambiguities, the production rate

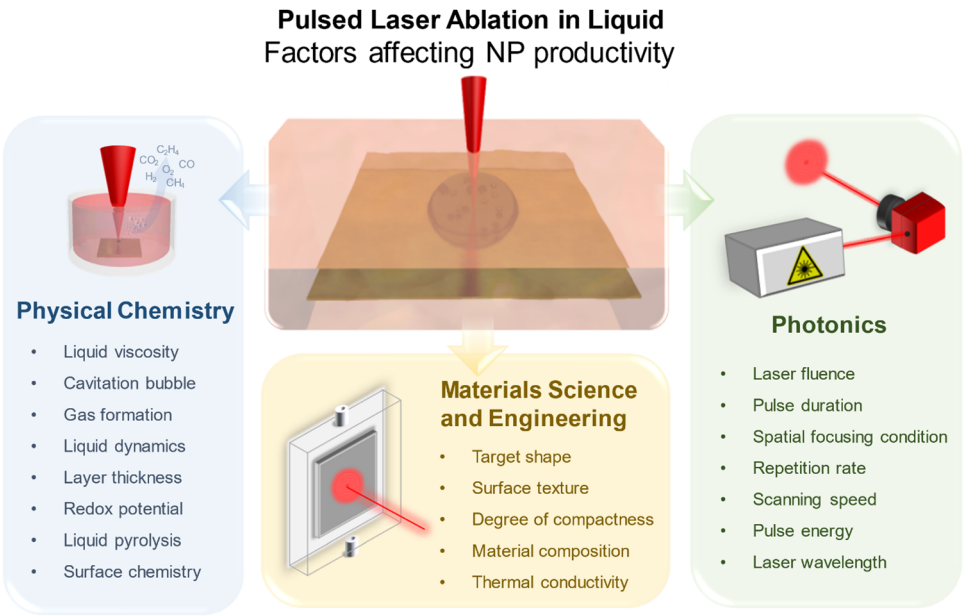

Fig. 1 A schematic illustration of PLAL depicting the laser-irradiated target immersed in a liquid and the factors affecting nanoparticle productivity categorized by its respective scientific field.

or productivity will be defined. Afterward, the perspective aim will be to enlighten the reader by providing responses to the following fundamental questions defining PLAL productivity. How does the employed laser source influence the productivity in LAL? What physicochemical factors of the target and the solvent are influencing PLAL productivity? How do those factors correlate? What are the current and upcoming strategies to increase PLAL productivity to the demanded g h^{-1} scale?

2. The fundamentals of PLAL

The main tool of PLAL is a pulsed laser, that sends its laser energy in packages (pulses) with a certain pulse duration or pulse width (τ_{pulse}). The average power and peak power of a pulsed laser can be calculated with eqn (1) and (2), respectively.

$$\bar{P}(\mathrm{W}) = E_p(\mathrm{J}) x f(\mathrm{Hz}) \quad (1)$$

$$P_{peak}(\mathrm{W}) = \frac{\bar{P}(\mathrm{W})}{f(\mathrm{Hz}) \times \tau_{pulse}(\mathrm{s})} = \frac{E_p(\mathrm{J})}{\tau_{pulse}(\mathrm{s})} \quad (2)$$

where $\bar{P}$ is the average power of the laser, P_{peak} is the peak power, f is the repetition rate or number of pulses in one second, τ_{pulse} is the pulse width or pulse duration, and E_p is the pulse energy. The peak power is inversely proportional to the pulse width, hence, the shorter the laser pulse duration the larger the peak power. In comparison to continuous wave lasers, pulsed lasers with the same average power can reach a significantly higher peak power, making laser ablation more efficient by reducing material heating.

The process of material removal and nanoparticle formation in PLAL involves a series of complex physical and chemical interactions between the material, the laser, and the liquid.[55–59] The interaction between the laser beam and the target induces a fast phase transition between the target-liquid boundary, leading to the formation of high pressure, temperature, and density plasma containing ionized and atomized species.[33,60,61] As the plasma decays at a fast-cooling rate, the surrounding liquid absorbs the energy and it is transformed into a layer of supercritical vapor containing the evaporated and dissociated species from the liquid, namely the cavitation bubble.[62] The cavitation bubble is presumed to be the reservoir of solid crystallization, *i.e.*, the formation of the atomic cluster, and primary and secondary particles.[63–65] The cavitation bubble might undergo expansion and shrinkage[65] before its final collapse, which releases the NPs to the surrounding liquid.[58]

Depending on the operating laser pulse duration τ_{pulse}, the ablation mechanism differs as shown in Fig. 2.[61] When a nanosecond laser is employed, the bulk target absorbs the energy and transfers it to the lattice, inducing energy release by heating the target, which causes melting, vaporization, bond-breaking, or defects formation that leads to material removal. All these processes take place while the laser is still irradiating the target. Meanwhile, when ultrashort pulses are employed (in pico- or femtosecond regime), the heating, melting, and material removal occur at a different time frame due to the electron–phonon coupling time being longer than the laser pulse duration. These differences due to the pulse duration

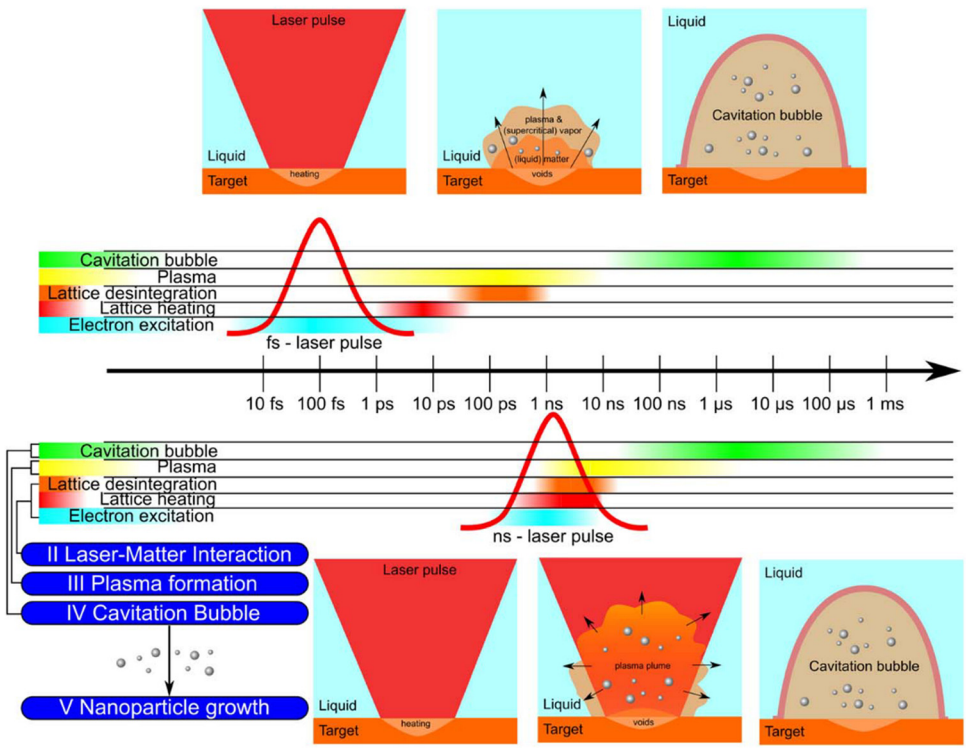

Fig. 2 Schematic illustration of the laser ablation occurring after pulse irradiation of the bulk target immersed in a liquid for femtosecond (top) and nanosecond (bottom) PLAL. Reproduced from ref. 61 with permission from IOP Publishing Ltd, copyright 2019.

influence the lifetime and cooling rate of the plasma, which leads to a unique plasma–liquid interaction, and thus, nanoparticle phase, size, and composition.[61]

A deeper understanding of the processes occurring at the time scale that goes from the pulse interaction with the material until NP ejection would help to select the optimum experimental parameters for every material and liquid.[66–68] This fact could lead to the desired nanoparticle's size, shape, composition, and surface coating, for example, the formation of CoFe layered double hydroxide from the sequential ablation of Co and Fe target in low concentration of $(NH_4)_2CO_3$,[69] which unlocks potential applications of laser-generated NPs in catalysis,[70] medicine,[71] additive manufacturing,[72] and energy generation and storage.[73] Nonetheless, productivity has been always one of the main limitations of the application of laser-synthesized NPs. Their outstanding properties have been mainly directed to applications demanding reduced NPs quantities due to the low yield. Consequently, the search for novel configurations and laser sources that permit an improved efficiency of the process, as well as productivity increase, has been one of the main research lines in the past years.[53,54,74–76] Nowadays, it still represents a major goal of the field.

3. Definition and measurement of nanoparticle productivity

The amount of NPs produced within a certain period of time is defined as the production rate or productivity. Its value commonly lies within the milligrams per hour range, meanwhile, it is important to achieve NPs productivity in gram per hour scale to popularize this technology, reduce cost and move toward industrial applications.

There are several strategies that can be employed to measure the ablated mass: (1) gravimetric, (2) optical extinction, and (3) analytical chemistry approaches.[77] In the gravimetric approach, the mass difference of a target before and after PLAL is measured to be the total mass of NPs produced. A high precision balance is usually employed, and the target should be dried from the liquid beforehand to reduce artifacts in the measurement due to the extra weight from the remaining liquid. The advantage of this approach is the easy and undemanding labor, but is not suitable for low productivities below the balance detection range, and the target mass difference can differ from the amount of colloidal nanoparticles produced if larger fractions of the target are ablated. This is especially relevant for powder-pressed targets where the compactness and porosity facilitate the detachment of larger particles by the laser action. The second approach, optical extinction, employs a spectrophotometer at the wavelength range between 200–1000 nm to measure the intensity difference of light passed through the liquid used as a reference compared to the colloidal NPs. Based on the Lamber-Beer law, the absorbance of a dissolved substance is correlated with the colloid concentration.[78] Hence, the absorbance of the dispersed NPs in the liquid can be linearly correlated to its concentration after a calibration of the spectrophotometer for the given material and solvent. It should be noted, however, that the concentration determination could only be applied if extinction (which consists of absorbance and scattering) is dominated by absorbance and the scattering effect is insignificant. If the scattering effect is significant, for example, in the case of big NPs sizes, the absorbance and scattering elements should be separated before one can determine the concentration through the extinction method. In addition, size-dependent effects due to plasmonic absorption cause a wavelength shift depending on the particle size which may affect the calibration.[79] Therefore, it is suggested to build two types of calibration curves: (1) at the peak wavelength of the surface plasmon resonance as a function of nanoparticle size[80] to estimate the size and simulate by Mie theory if the scattering should be considered or can be avoided, and (2) at a wavelength outside of the plasmon of resonance where we have a linear dependence of the absorbance with the concentration. Once the calibration curves are obtained, this approach is more efficient than the gravimetric method since the target does not need to be removed and placed for each measurement. The drawback of this approach is the unreliability for colloids at extreme concentrations (too high or too low) and materials which easily agglomerate and sediment, such as magnetic NPs.[81–83] In the case of highly concentrated colloids where the high absorption obscures the characterization, dilution of the colloid can be employed to reduce agglomeration effects. Furthermore dilution increases colloidal stability while bringing the absorption value to the linear regime of the concentration calibration curve without reducing the resolution of the concentration determination. Meanwhile, the approach to use analytical chemistry techniques usually requires a dilution of the sample, for instance, the inductively coupled plasma mass spectrometry (ICP-MS), as the system is well suited for very low concentrations. These techniques can be used to provide the calibration curve required for optical extinction spectroscopy. The drawback of this approach comes from the high price of the equipment and the possible inaccuracies in the dilution process.

To obtain a reliable value of the gram per hour productivity in an experimental procedure, long irradiation times of 1 hour could be required to showcase the robustness and reliability. Nevertheless, the productivity is commonly obtained by extrapolating the ablated mass in minutes to one hour. Please note that in this situation some factors that may affect the productivity, *i.e.*, nanoparticle shielding, permanent bubbles, and successive irradiation of the same area of the target, maybe neglected in the extrapolation. For this reason, the minimum ablation duration of 5 minutes is required to obtain a reliable gram per-hour value while also accounting for the effect of nanoparticle shielding,[76] target depth variation, persistent microbubbles,[84] and scanning and repetition rate effects.[54] It has been shown that there is no major discrepancy in the productivity between 5, 10, 15, and 30 minute ablation time when using a flow chamber.[53] Please note that depending on the ablation chamber, an extrapolation from 5 minutes of ablation to 1 hour ablation might not be accurate. For example, colloidal concentration saturation (indicated by low transparency) will be reached faster if the ablation is done in a batch chamber with a

smaller liquid volume, leading to an ineffective ablation and lower productivity overtime, thus, inaccurate results when extrapolating from shorter ablation time to long term ablation. Therefore, it is recommended to use a flow chamber with an optimum flow rate and a constant feed of fresh liquid to avoid colloidal concentration variation over time.

Other than the aforementioned mass per time unit (mass productivity), we can also define productivity by the laser parameters or material properties, such as laser power and material density. Dividing the value of mass productivity by the laser power results in ''power-specific productivity'' with a unit of mg h^{-1} W^{-1}, which defines the efficiency independent of the laser power used to produce the NPs. Since the laser sources employed in PLAL differ from one lab to another, it represents a comparable value to facilitate the repeatability of the process, however, other key laser parameters such as the pulse duration, repetition rate, and scanning speed have to be considered when transferring results to a new setup.[85] The density-dependent productivity is obtained by dividing the mass productivity by the material density. Therefore, it is also called ''volume productivity'' (usually provided as mm^3 h^{-1}). This approach is useful to compare the productivity of different materials with different densities since high-density materials usually show higher mass productivity compared to low-density materials.[86] Another way to define productivity is the ''molar productivity'', obtained by dividing the ablated mass by the molar mass of the material, which gives out the final units of mmol h^{-1}. Since the unit is in mole (defining a number of 6.022×10^{23} ions, atoms, molecules, *etc.*) instead of molar (mole per liter), the terminology of ''mole productivity'' would be more appropriate. This terminology describes the number of atoms ablated from a target within a period of time, which might be useful in the field of reactive laser ablation in liquid to determine the stoichiometric reactant amount and study its influence on the generated phase of the NPs or the gas composition.

Despite many terminologies used to evaluate and define the productivity of a PLAL system, there are too many factors influencing this complex system. It is therefore implausible to define only one measurement technique and one unit as a standard in PLAL. The chosen measurement technique and the unit will then depend on the feasibility of the experimental procedure in the laboratory and the focus of the research itself, whether it is to compare the productivity of different materials or to compare a common material irradiated with different laser systems. For the goal to scale-up PLAL and reach an industry-relevant production, the simplest way to define the productivity is the gravimetric approach combined with well-calibrated optical spectrophotometry characterization of the colloids to confirm the absence of large fractions of the target. This way, it is possible to achieve good repeatability and accuracy of the method, especially for large production of NPs.

Once the PLAL principles have been introduced, and the productivity has been defined, the influence of the laser and material parameters on productivity and strategies to increase productivity will be discussed. In order to achieve the gram per hour productivity, approaches such as developing new types of chambers,[74,87–89] bypassing the cavitation bubble,[52,90] and reducing the liquid layer thickness,[88,91] have been sought. In the following chapter, we will discuss the parameters related to the NPs productivity starting from the laser fundamentals, *i.e.*, laser fluence, pulse width, and laser wavelength, to the practical point of view including the chamber design and target geometry.

4. Strategies to increase nanoparticle production

The benefits from employing laser-synthesized nanomaterials for catalysis,[10–12,69,70] biocidal elements,[92,93] bioimaging,[94] and modification of material properties such as the absorption for additive manufacturing[95] has already been proven. Nevertheless, these processes demand not only large amounts of nanoparticles but also cost-effective production processes. As lasers are easily integrated into the production chain and their industrial use is widely extended, the incorporation of PLAL is straightforward.[96] The development of higher production and cost-effective processes to boost the employment of laser-generated nanomaterials at a large scale represents one major challenge that researchers working in this field are facing nowadays.[97]

A first thought on the possibilities for increasing productivity in PLAL immediately leads to the study of laser-matter interaction. The first approach that can come to mind is to optimize laser parameters by increasing laser power and repetition rate, and find the optimum irradiation wavelength for the employed material. Nowadays, there exist commercial laser systems operating at wavelengths from the UV to the IR able to achieve mean power values of hundreds of Watts that allow obtaining huge fluence values at the focal spot even operating at repetition rates in the order of the MHz. However, above a fluence threshold, limitations that depend on the scanning velocity,[52] repetition rate,[53] pulse width,[68] focusing conditions,[98] interaction with the liquid media,[99] and target geometry appear.[100] Consequently, several parameters are involved, and their optimization turns into a difficult task that even varies depending on the material, liquid, and pulse duration.

4.1. Finding the optimal laser fluence and pulse duration

A fundamental parameter for nanoparticle production is laser fluence. Its influence can be explained starting from the well-established model for material processing in air.[101,102] Depending on the pulse duration, the ablation mechanism differs. In the case where pulse duration is shorter than the electron cooling time, typically pulses shorter than 1 ps, the strong evaporation regime is produced and material removal is associated with the direct solid–vapor or solid–plasma transition, avoiding melting of the material. If the pulse duration exceeds the electron cooling time, the released heat causes first the melting of the material surface and its posterior vaporization or solidification. Following the results obtained by this model,[101–103] the ablation depth (L) can be described in terms of the fluence:

$$L = \delta \cdot \ln\left(\frac{\phi_{inc}}{\phi_{th}}\right) \quad (3)$$

$$\phi_{inc} = \frac{2E_p}{\pi w_0^2} \quad (4)$$

Here, δ is the effective penetration depth, ϕ_{inc} is the incident fluence on the target (which can be calculated by eqn (4)), ϕ_{th} is the threshold fluence, E_p is the pulse energy, and w_0 is the beam half-waist (spot radius). This model of laser ablation in air can be used to explain the relationship between ablated volume per pulse and fluence by assuming a Gaussian-shaped laser intensity profile. Integrating eqn (3), then substituting beam waist w_0 with incidence fluence ϕ_{inc} based on eqn (4), to get eqn (5). The derivation of this equation can be found in the ref. 104 and 105. Please note that this equation cannot be directly implemented for PLAL, as the presence of the liquid causes non-linear interactions, absorption, as well as scattering, and shielding due to the cavitation bubble and generated NPs. Nevertheless, this equation will help to understand the relationship between ablated volume and incident fluence, which is an important parameter in PLAL.

$$V = \frac{E_p}{2\phi_{inc}} \cdot \delta \cdot \ln\left(\frac{\phi_{inc}}{\phi_{th}}\right)^2 \quad (5)$$

From eqn (5), the ablated volume per pulse exhibits a logarithmic relationship with the incident fluence; the higher the fluence, the larger the ablated volume per pulse. The incident fluence can be increased by focusing the laser beam, increasing the laser power, and reducing the repetition rate (to increase the pulse energy). The fundamental parameter defining the ablation process regime is the threshold fluence (Fig. 3). When the incident fluence is below the ablation threshold, the NP yield is negligible. When the incidence fluence reaches the ablation threshold, the ejection of matter increases significantly by more than one order of magnitude.[106] After overcoming the ablation threshold, increasing the incident fluence has a lower effect on the ablation yield, and the ablation volume is determined by the effective penetration depth.[105]

Above the ablation threshold, the effective penetration depth is a key parameter to increasing the ablation volume. The penetration depth of a material is influenced by the pulse width and the materials' properties, such as reflectivity, absorbed wavelength, and surface structure. An increasing pulse width results in a decrease in the penetration depth.[107,108] The penetration depth can be classified into optical penetration depth and thermal penetration depth. The optical penetration depth dominates in the low fluence, ultrashort pulsed lasers (<1 ps) regime because the pulse duration is shorter than the electron cooling time, avoiding energy dissipation through heat transfer to the target materials. Reduction of target heating results in a more efficient ablation. Meanwhile, the thermal penetration depth is the dominating factor for longer pulses (≥ 20 ps). When the pulse duration is longer than the electron–phonon relaxation time, usually a few picoseconds for metals,[55] the energy received by the material will be dissipated to the atom lattice of the material as heat and subsequent melting, leading to a lower process yield.

In addition to the penetration depth, the ablation threshold is also affected by the pulse width. A simulation for a 150 ps laser *versus* a 15 ps laser (Fig. 3),[106] found that the ablation threshold is $\sim$20% higher for the longer pulse width (35 J m^{-2} at 150 ps) than the shorter pulse width (29 J m^{-2} at 15 ps). It is also reported that the ablation yield of the 15 ps laser pulse is constantly higher at all fluences above the ablation threshold compared to the 150 ps laser. Meanwhile, if the ablation is performed at a fluence lower than the ablation threshold, the pulse duration does not change the yield of the ejected species.[106] Experimental results confirm the ablation threshold variation with the pulse width (100–4500 fs) for copper, aluminum, and steel.[109]

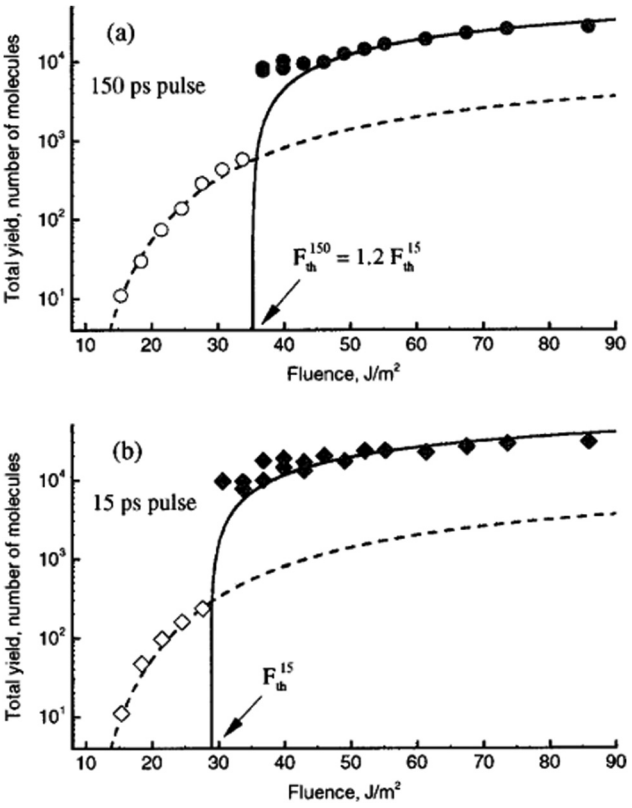

Fig. 3 Simulation of laser ablation of organic solids at different fluences using two different pulse widths. Hollow data points represent the ablation regime below the ablation threshold and the filled data points denote the ablation at or above the ablation threshold. The graphs show that the ablation using a shorter pulse width resulted in a lower ablation threshold fluence. Reproduced from ref. 106 with the permission from AIP Publishing, copyright 2000.

Based on the above discussion, we might consider using ultrashort pulse lasers (femtosecond lasers) over picosecond and nanosecond lasers for a higher production rate. Nevertheless, the influence of pulse width on NP productivity by PLAL is not only the ablation threshold reduction as in air, but also peak power and intensity-dependent interaction of the pulses with the liquid.[110–113] Picosecond lasers are found to provide a suitable subcritical peak pulse power for the ablation process in the liquid medium, thus, generating the highest NPs yield per pulse and per unit energy.[112] The ultrashort femtosecond lasers, on the other hand, trigger non-linear optical absorption, self-focusing, and filamentation effects in the liquid medium as it reaches supercritical peak pulse power, which affects the beam spatial profile and generates energy losses, decreasing the overall

productivity.[112,114] The same trend is also observed for longer pulse duration in the nanosecond regime, in which plasma screening is attributed to be the main cause of productivity reduction, besides the energy loss from thermal processes such as localized heating and melting.[112] It has been suggested that the use of picosecond lasers is advantageous compared to femtosecond lasers if the generated thermal energy can be redistributed, *i.e.*, by using a liquid flow ablation chamber.[114]

Regarding the efficiency of ns and ps PLAL, a study by Kohsakowski *et al.* (2018)[115] compared the mass-, power-, and investment-specific productivities of three different laser systems for the ablation of gold, platinum, silver, and nickel in water. In terms of absolute productivity depicted as mass per unit time, (Fig. 4a), the picosecond laser system supported by the 500 m s^{-1} scanning speed polygon scanner[52] achieved the highest value compared to the nanosecond laser system. Nevertheless, as the use of a polygon scanner reduced the laser power reaching the target by half, thus the power-specific productivity is also reduced by half, making clear that the scanning technology is one of the main limits to overcome the barrier of PLAL productivity. For gold and silver, the power-specific productivity is lower for the picosecond laser compared to the 10 ns-laser, while it is almost similar for platinum and nickel (Fig. 4b). In addition, the investment-specific productivity, which defines the mass of generated NPs divided by time and investment cost (Fig. 4c), showed that the 10 ns-laser performed better than the 3 ps-laser for gold and silver NP production by 11% and 15% in every 1000 € investment, respectively. The absolute power and investment-specific productivities confirm that longer pulses, 40 ns laser source, lead to lower productivity due to thermal interactions and plasma shielding. Although the investment-specific productivity depends on the target material, from the economic point of view, the consideration of laser power and investment cost is crucial as even a small difference can turn into a significant profit in the long run. In addition, the lower initial investment cost of the 10 ns-laser at around 100 000 €, compared to the approx. 500 000 € for the 3 ps-laser, enables small-scale industries to begin investing in this green method to produce NPs. Furthermore, both ns and ps lasers can be complementary in terms of producing different material phases, core–shell structures, or composites, making productivity upscaling relevant in both cases.

The fluence defines the ablation regime, and the pulse duration has been proved to play a key role by influencing the threshold fluence of the material and the intensity that determines the interactions with the liquid. However, the pulse duration is not the only important factor to define the intensity and fluence of the laser beam interacting with the liquid and the target. The spatial focusing conditions define the incident fluence and laser intensity during propagation, influencing PLAL productivity. Placing the focal spot in front of the target, *i.e.*, in the liquid, leads to the laser mainly interacting with the liquid in front of the target, inducing liquid breakdown and scattering of the incoming laser beam. Depending on the laser wavelength, focusing the laser beam in the liquid may also induce fragmentation of the generated NPs that shield the laser beam energy from reaching the target.[76] Placing the focal spot

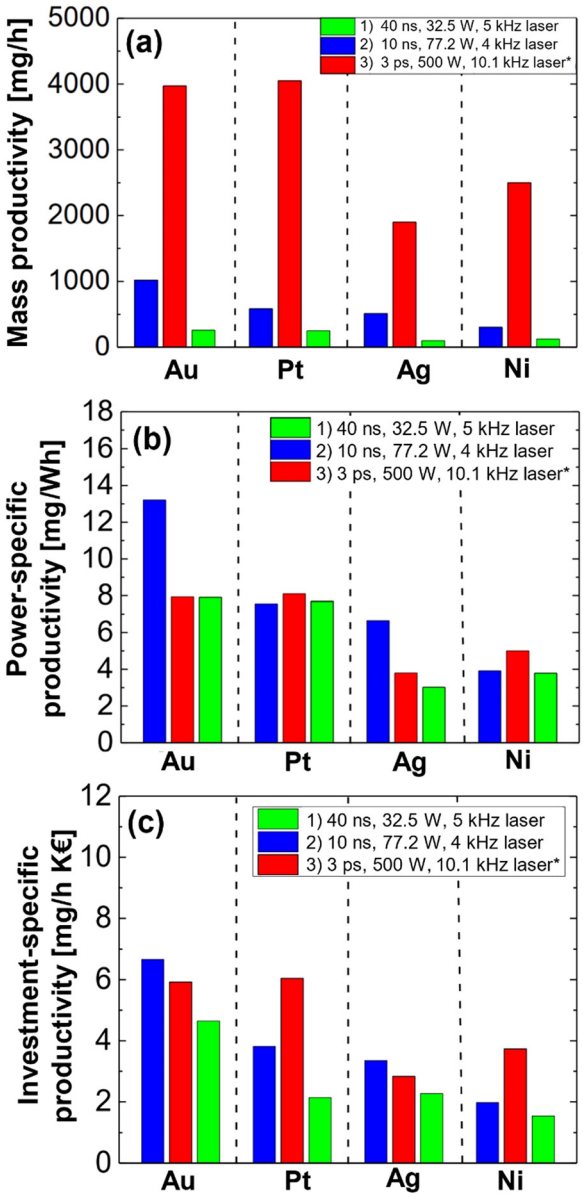

Fig. 4 Productivity comparison of three different laser systems for the ablation of Au, Pt, Ag, and Ni in water, adapted from ref. 115 with permission from author, licensed under CC BY 4.0, copyright 2018. Each figure indicates a different productivity calculation approach: (a) mass productivity, (b) power-specific productivity, and (c) investment-specific productivity. The asterisk (*) indicates that the data is reproduced from ref. 52 with permission from IOP Publishing Ltd, copyright 2016.

on the target surface is usually preferred to maximize the laser fluence and get the maximum ablated volume. Nevertheless, Waag *et al.*[75] suggested that placing the focal spot slightly behind the target (0.7–4.7 mm) increases NP productivity compared to placing the focal spot on the surface of the target (0 mm) (Fig. 5). The authors argue that the highest productivity does not occur at the focal spot due to the minimized spot area of the laser, which would be equivalent to performing the process with a longer focal length or smaller diameter of the laser beam before the lens. Thermal analysis of the liquid and the target revealed that the target reached the minimum heating

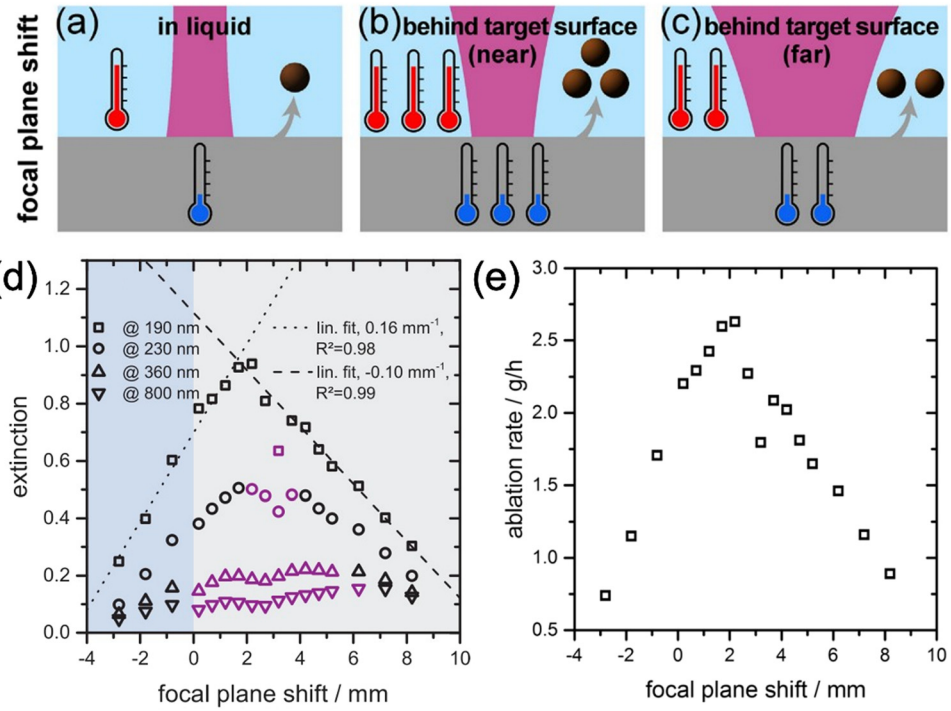

Fig. 5 Schematic illustration of how different focusing conditions affect the productivity: (a) focal spot on the liquid resulted in the lowest productivity, (b) focal spot behind the target (near, 2 mm) resulted in the highest productivity, and (c) focal spot behind the target (far) resulted in the moderate productivity. Ablation rate results are based on (d) extinction approach and € gravimetrical approach. Adapted from ref. 75 with permission from Elsevier, copyright 2019.

while the colloid reached the highest temperature under the experimental conditions proposed. The temperature distribution in the liquid and target is explained by the reduction of heating effects by the proposed laser defocusing. The high temperature of the liquid is caused by the heat released from the larger number of generated NPs.[75] Later results confirmed that the material removal rate can be maximized by changing the focusing conditions and varying the size of the beam waist.[104]

Overall, the spatial focusing conditions influence PLAL productivity by affecting the fluence and intensity profile of the beam at the focal spot and propagation through the liquid. The focal length and beam diameter, directly affect the numerical aperture and focal spot size, which completely modifies the laser intensity during propagation as well as the fluence. The optimum focal length and beam diameter depend on the target due to the differences in the threshold fluence between materials, the liquid due to the nonlinear threshold fluence and intensity, and the pulse duration. The modification of the focal length within a PLAL system is many times unfeasible since fast galvanometric scanners are employed, and the f-theta lens exchange requires an economical investment and sometimes difficult modification of the chamber positioning. Consequently, for PLAL systems with fixed optics, defocusing the beam appears as a straightforward solution to achieve the optimum processing fluence.

4.2. Taking into account the nonlinear effects

The impact of pulse duration on the primary mechanism of laser material removal has been previously discussed. Furthermore, the width of the laser pulse, which affects peak power and intensity, has been shown to have an impact on PLAL through its influence on parameters such as cavitation bubble properties, absorption, scattering, and target temperature. For example, experiments on the laser ablation of metal targets in air showed that material removal efficiency is increased as the employed laser pulse width is shorter,[116,117] due to the reduced thermal interaction and more efficient use of the energy for material removal process.[114,118,119] This evidence points towards femtosecond lasers as an ideal tool for efficient material removal.

However, the nonlinear interactions that dominate the ablation process at the femtosecond time scale also represent a source of energy losses due to the generation of these phenomena in the liquid prior to the interaction with the target.[120] Besides, nonlinear effects like filamentation and self-focusing not only produce energy losses but also modify the divergence of the beam and so the focal spot position.[98] This variation alters the ablation fluence if the target is not conveniently realigned and complicates the reproducibility of the experiment.[98] This fact is even more critical considering that the modification of the focal spot position is power dependent, and so a variation of the laser energy turns into a shift in the focal spot location.[121] It should be noted that the appearance of this phenomenon is not only related to the laser pulse width but also to the laser peak power and intensity.[112] The frontier between linear and nonlinear effects predominance is generally assumed to be in the limit between ps and fs timescales.[113,122] Nevertheless, parameters related to the material and laser properties should be considered for every specific situation to obtain the threshold value and evaluate the optimum experimental conditions.[99]

The limitations related to the presence of a liquid medium and energy losses due to the generation of nonlinear effects restrict the application of fs lasers for nanoparticle production upscaling.[123] Then, as an intermediate solution to decrease thermal interaction while avoiding strong nonlinear interactions, ps lasers are commonly employed when production upscaling is desired.[74] Nevertheless, effective control of nonlinear effects produced in the liquid media is a promising path towards PLAL production increase by the employment of high power and high repetition rate femtosecond lasers. Recently, the Simultaneous Spatial and Temporal Focusing (SSTF) technique has been proposed in PLAL as an alternative to conventional single-lens focusing to address the problem of energy losses due to the nonlinear effects interaction of femtosecond pulses propagation through the liquid layer. The key idea of the SSTF system is that a diffractive grating provides a spatial chirp to the femtosecond beam, so the different spectral components are separated and only recombine at the spatial focus of the objective lens (Fig. 6a). This produces a significant increase in the pulse width during its propagation in the liquid and, consequently, the reduction of the nonlinear losses. However, thanks that the grating is imaged into the sample by means of an optical setup, the original femtosecond pulse width is recovered over the target so keeping the desired high-efficiency ablation of femtosecond pulses. This strategy for beam delivery allows a reduction of a 70% factor of the nonlinear energy losses compared to the standard fs PLAL system, resulting in a productivity increase of 2.4[99] (Fig. 6b).

4.3. Reducing liquid and nanoparticles absorption and scattering *via* laser wavelength selection

Nonlinear effects are not the only interaction with the liquid that influences productivity, linear interactions such as absorption, reflection, and scattering occurring both in the liquid and the target need to be accounted for to maximize PLAL NPs yield. The laser wavelength defines these processes, as each material's absorption, reflectance, and scattering depend on the wavelength of the incident light.[124–126] Higher absorption of the target at the laser wavelength leads to a higher energy density delivered to the sample and so the ablated volume increases. For example, for laser ablation in air, if a material has a low absorptivity at 1064 nm, the amount of ablated material with an Nd:YAG 1064 nm laser will be lower.[126]

The optimum processing wavelength of the material can be determined by spectrophotometry, hence defining the most suitable wavelength for laser ablation in air. Nevertheless, the absorption of the liquid and generated nanoparticles in the laser ablation in liquid produce energy losses, requiring a laser wavelength with low liquid absorption and high material absorption.[127,128] This key difference with ablation in air is shown in materials such as Au and Ag where the maximum ablation efficiency laser wavelength differs from ablation in air.[129,130] Scattering and inter- and intra-pulse absorption are commonly found as the main hurdles to increasing PLAL productivity. Intra-pulse absorption is related to the laser pulse width, which is found for longer pulses in the ns regime and above, as the pulse tail can be absorbed by the generated NPs and plasma plume from the pulse front.[127] The scattering and inter-pulse absorption, on the other hand, are associated with the extinction coefficient of the liquid and the generated colloidal NPs, which affect the laser energy delivered to the target.

As reported by Intartaglia *et al.* (2014),[131] the ablation of Si in water using a UV laser (355 nm) resulted in lower productivity compared to the ablation using a NIR laser (1064 nm) as shown in Fig. 7. They observed two different regimes in the UV laser ablation, termed transient and steady-state regimes, where the productivity is higher during the transient regime (smaller number of pulses, shorter ablation time) compared to the steady-state regime (larger number of pulses, longer ablation time) (Fig. 7b). TEM analysis shows that the smaller Si NPs size is obtained with increasing ablation time, proving the photofragmentation phenomenon.[131] Meanwhile, the ablation using a NIR laser (Fig. 7a) shows a steady ablation yield and the particle size is also bigger than the UV-ablated Si NPs. These effects are especially prominent if a batch chamber is used in PLAL, where the generated NPs stay in the chamber after the

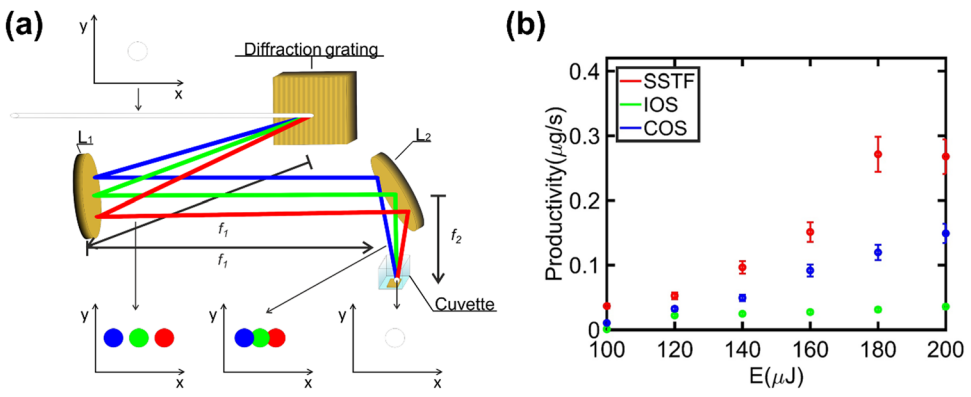

Fig. 6 (a) Experimental setup of the fs SSTF-PLAL system based on the spatial separation of the spectral components of an fs pulse that is only recombined at the focal spot, returning to the initial fs pulse duration. (b) NP productivity as a function of the pulse energy for the fs SSTF-PLAL, standard fs PLAL (COS), and analogous system to fs SSTF-PLAL without spatial separation of the spectral components (IOS). Reproduced from ref. 99 with permission from Chinese Laser Press, copyright 2019.

generation and shield the laser beam. The employment of a flow chamber is thus recommended to reduce scattering and absorption related to the generated NPs and to improve the productivity. Selecting the laser wavelength with minimum absorption and scattering by the generated NPs is crucial to maximizing the laser energy delivered to the target. While UV laser is more beneficial to produce smaller NPs due to the fragmentation effect, the NIR laser is the most ideal choice to obtain high ablation yield due to the low absorption by generated NPs.

4.4. Bypassing the cavitation bubble

The optical phenomena occurring in the liquid are not the only difference between laser ablation in air and PLAL. The presence of the liquid and the laser interaction promotes the formation of a cavitation bubble for each pulse interacting with the target. This vapor bubble is formed when the local pressure drops below the liquid's vapor pressure; hence, the inside of the bubble is filled with vapor. The cavitation bubble in PLAL is formed due to the instant vaporization of the liquid exposed to the heat of the plasma plume. The temperature of the plasma plume was measured experimentally by capturing the optical emission intensity of the plasma during the ablation of a target using an ICCD camera with a resolution of 50 ns.[60,132–135] The obtained continuum spectra are fitted to the Planck equation to obtain the plasma plume temperature.[136,137] The ablation of materials in water is reported to generate plasma plumes with a temperature in the range of 4000–8000 K.[132,133,135,137] Meanwhile, another study of graphite ablation in water with a 5 ns resolution shows a maximum plasma temperature of 25 000 K, which reached 20 ns after the laser pulse interaction.[138] After the cavitation bubble formation and expansion up to the maximum height, the cavitation bubble undergoes a shrinkage process and finally collapses, releasing a shockwave to the surrounding liquid. The lifetime and maximum height of a cavitation bubble depend on many factors, including laser fluence,[76] pulse width,[76,139,140] number of irradiated pulses at the same spot,[141,142] liquid density,[143] the thickness of liquid layer,[144] liquid viscosity,[145] target geometry,[100] and liquid compressibility.[146] Its maximum height varies strongly with the pulse width, ranging from tens of μm as in femtosecond tissue ablation,[139] to several mm in nanosecond ablation of alumina.[140]

The cavitation bubble's lifetime and size strongly constrain PLAL productivity. In continuous ablation PLAL, the first bubble generated by the first laser pulse can shield the subsequent pulses, hindering the laser energy that reaches the target material. Two strategies have been proposed to bypass the cavitation bubble (Fig. 8a). The first one is to temporally bypass the cavitation bubble, which means that the subsequent pulse is sent when the previous cavitation bubble already collapsed.[90] This approach is only suitable for low repetition rate laser sources, for example, if the lifetime of the cavitation bubble is 100 μs, the maximum repetition rate that can be employed is 10 kHz to temporally bypass the cavitation bubble.[147] Nevertheless, high repetition rate lasers with high pulse energy are desired to increase PLAL productivity. Hence, the second proposed mechanism, *i.e.*, spatially bypassing the cavitation bubble, represents a more feasible way to achieve industrial-scale PLAL production. Spatial bypassing of the cavitation bubble can be achieved by a high scanning speed of the processing pattern. The distance

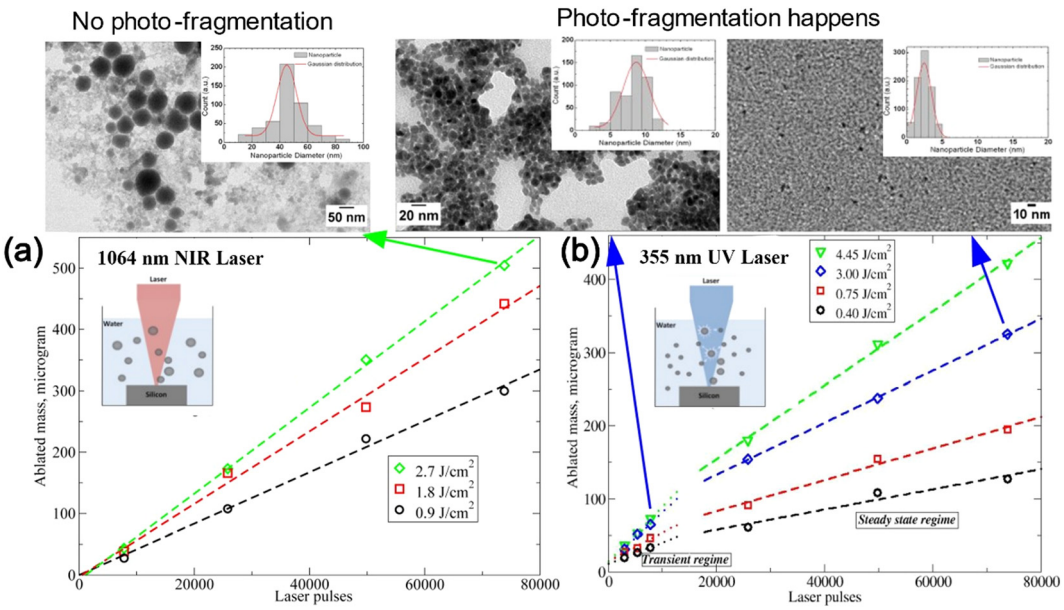

Fig. 7 Laser wavelength influence on the productivity and particle size of Si ablation in water. (a) Ablation using a 1064 nm NIR laser shows steady ablated mass as a function of a number of pulses (ablation time) in different fluences. The inset, indicated by the green arrow, shows the TEM image and particle size distribution of Si ablated using a 1064 nm NIR laser. (b) Ablation using a 355 nm UV laser produces smaller Si NPs with increasing ablation time due to photo-fragmentation. Insets, indicated by the blue arrows of the respective data point, show the TEM image and particle size distribution of Si ablated using a 355 nm UV laser. Adapted from ref. 131 with permission from The Optical Society, copyright 2014.

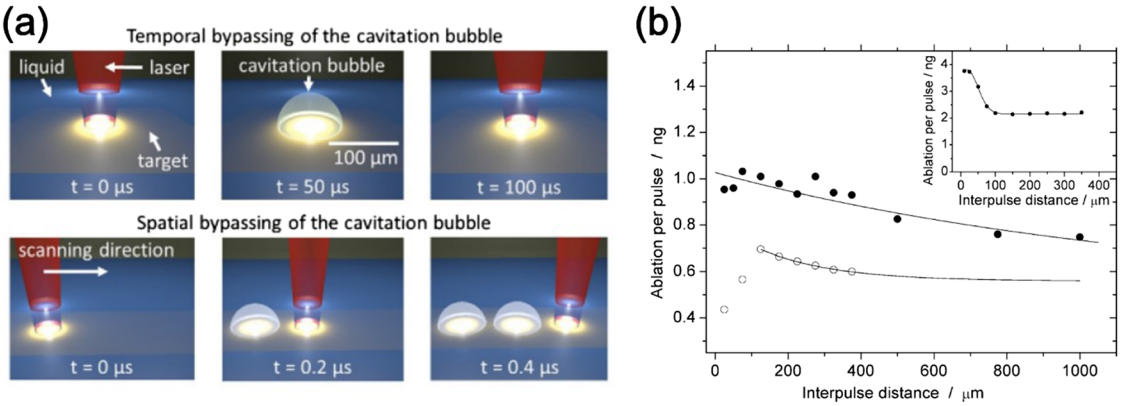

Fig. 8 Bypassing the cavitation bubbles. (a) Schematic representation of temporal and spatial bypassing of the cavitation bubble (reproduced from ref. 74 with permission from The Optical Society, copyright 2016) and (b) ablation per-pulse of Zn in tetrahydrofuran as a function of the interpulse distance, depending on the bypassing mechanism. Filled data points are temporal bypassing by using a low repetition rate (1 kHz), while hollow data points represent spatial bypassing (repetition rate of 10 kHz). The inset shows the ablation per pulse of the Zn target in air. Adapted from ref. 90 with permission from American Chemical Society, copyright 2010.

between pulses has to be at least equal to the cavitation bubble radius so the subsequent pulse does not interact with the bubble formed by the previous pulse. The suitability of this approach for PLAL production upscale was confirmed by Wagener *et al.* (2010),[90] comparing the productivity of Zn ablation in tetrahydrofuran (THF) varying the inter-pulse distance and repetition rate to study the influence of temporal and spatial bypassing of the cavitation bubble in picosecond PLAL.[90] In their setup, the inter-pulse distance was kept constant for different repetition rates, maintaining the number of pulses irradiation of the sample (10^6 pulses) to obtain comparable productivity values. At 10 kHz, increasing the inter-pulse distance up to 125 μm enhanced the ablation efficiency. Then, a gradual decay of the ablation rate is observed (Fig. 8b, hollow data points). The initial productivity increase is related to the spatial bypassing of the cavitation bubble combined with the incomplete thermal relaxation of the material irradiated by the previous pulse, leading to trapped heat and a phase explosion as the dominant ablation mechanism. Contrarily, for inter-pulse distance larger than 125 microns, the irradiated area has not experienced heat accumulation due to the previous pulse, being thermal ablation as the main mechanism instead of phase explosion, and gradually lowering the ablation rate.[90] Temporal bypassing is achieved at 1 kHz, with a low productivity variation for lower repetition rates (Fig. 8b, filled data points). It is important to critically note that when evaluating the size and lifetime of cavitation bubbles with respect to productivity, the dimensions of a bubble induced by a single pulse are being considered. Nevertheless, it is known that these dimensions vary when multiple pulses hit a target.[142]

In a real NP production scenario, the laser power and repetition rates are maximized while keeping the optimum fluence in order to deliver the larger amount of pulses and maximize the ablated volume. In this scenario, a fast-scanning system is required to increase the inter-pulse distance and increase the ablated area to ensure that the target has enough time between successive scanning patterns to cool down. The scanning speed becomes a fundamental parameter together with the repetition rate and the cavitation bubble size for each specific system to ensure cavitation bubble bypass. As an example, for a cavitation bubble with an average radius of 100 μm produced with a laser source operating at a 100 kHz repetition rate, the minimum scanning speed required to completely bypass the cavitation bubble is 10 m s^{-1}. The galvanometer scanner technology can reach 10 m s^{-1}. Nevertheless, if the repetition rate is further increased to the MHz range, scanning speeds of at least 100 m s^{-1} are required. As the number of delivered pulses per second is critical for PLAL productivity, the required scanning speeds reach the current technological limitations.

The galvanometer scanners are based on the mirror(s) revolved with rotary motor(s) that deflect the input beam into a designed pattern with micrometric precision.[148] This working principle limits the maximum speed that can be achieved by this technology due to the inertia from the mass of the mirror(s) and other moving parts.[149] The fastest reachable speed of a galvanometer scanner is less than 200 rad s^{-1}.[150,151] If the scanner is paired with an f-theta lens with a focal length of 167 mm, the maximum scanning speed at the working field is approximately 35 m s^{-1}.[152] In 2013, De Loor introduced a new scanning technology based on the rotation of mirrors fixed on a polygon wheel.[150] The wheel rotates at a constant speed and the incoming beam is deflected on the flat facet of the mirrors (Fig. 9a). This polygon scanning technology offers a beam deflection speed of up to ~1000 m s^{-1}.[150,153] However, since the corner of the polygon wheel will deflect the beam at uncontrolled angles, the laser beam is shut off during this time and the laser beam only irradiates the target within a certain percentage of the duty cycle. This effect is more pronounced for small processing patterns, requiring large patterns with lower spatial resolution than the galvanometric scanners.[148] Streubel *et al.* (2016)[74] proposed for the first time the employment of a unidimensional polygon scanner (500 m s^{-1}) together with a galvanometric scanner to achieve a 2D scanning of the target sample (Fig. 9a). The fast scanning system was employed with a 500 W, 10 MHz, 3 ps laser source to maximize the number of

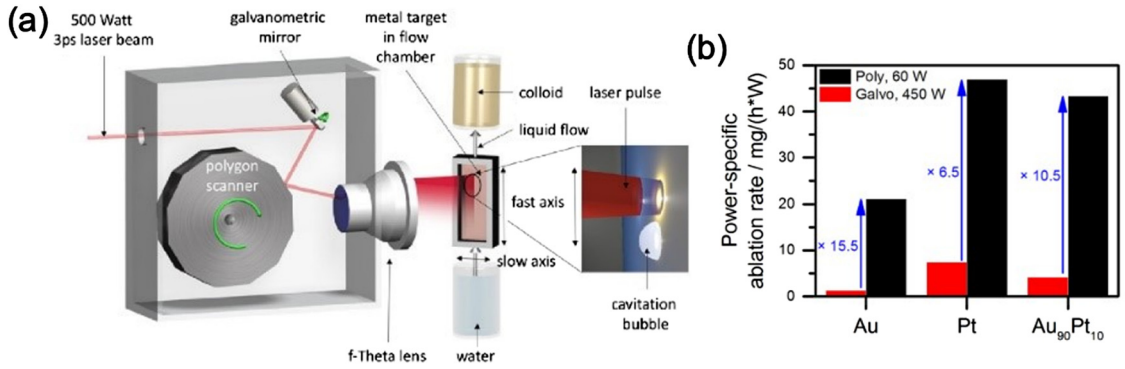

Fig. 9 (a) Schematic illustration of the ablation set-up using a polygon scanner (reproduced from ref. 74 with permission from The Optical Society, copyright 2016) and (b) power-specific ablation rate comparison of a galvanometer scanner (red) to the polygon scanner (black) for different materials (reproduced from ref. 54 licensed under CC BY 4.0, copyright 2021).

pulses per second by processing the target at 10 MHz achieving fluences above the threshold fluence thanks to the high power delivered.[74] The fast scanning speed allows the bypass of the cavitation bubble, reaching productivities as high as 4 g h^{-1} for PLAL of Pt. A direct comparison of PLAL with a galvanometric scanner (5 m s^{-1}) compared to the polygon scanner (484 m s^{-1}) resulted in a difference up to 16, 7, and 11 times for the ablation of Au, Pt, and $Au_{90}Pt_{10}$ targets, respectively (Fig. 9b).

In conclusion, PLAL upscaling requires faster scanning technologies. Using high-speed polygon scanners is one of the easiest ways to enhance NPs production.[154] However, their high prices, low precision demanding large scanning patterns, and their duty cycle that reduces the initial laser power employed in the target processing by a 50% factor, make it difficult the implementation of this technology in every PLAL system. Consequently, galvanometric scanners generally still represent more economical and repost alternative for PLAL, especially when fast galvanometric scanners reaching 30 m s^{-1} are employed.

4.5. Avoiding persistent microbubbles

The productivity of PLAL can be adversely affected not only by cavitation bubbles and NPs in the laser path but also by the formation of so-called persistent microbubbles during the ablation process. Persistent microbubbles are spherical and stable gas bubbles, generated from the collapse of the cavitation bubbles. While a cavitation bubble lifetime is approximately 0.1–1 ms,[145] persistent microbubbles can stay even as long as seconds.[135] Consequently, it is critical to understand the liquid, target, and laser processing parameters related to the lifetime of the persistent microbubbles in order to avoid their presence that shields the laser beam and can even become a safety issue when they stick to the chamber window, increasing reflectivity and even leading to glass breakage by the high-intensity laser source. Kalus *et al.* (2017)[145] investigated the formation of persistent microbubbles during the ablation of gold in 11 different liquids with various viscosity, as shown in Fig. 10a and b. The influence of the liquid viscosity over the amount, cross-sectional area, size, dwell time, and ascending speed of the persistent bubbles was evaluated. It was found that higher liquid viscosities increased the size and dwell time of the generated persistent microbubbles.[145] As shown in Fig. 10b, the ablation yield difference based on the liquid viscosity shows a factor 3 reduction when the ablation is done in liquids with a viscosity higher than 20 mPa s compared to liquids with a viscosity lower than 1 mPa s. A different study[86] revealed the influence of the target material over persistent bubbles generation. Different targets were irradiated in water and the gas formation (H_2 and O_2) was measured. The results show that less-noble metal such as Al produces the largest gas volume, followed by titanium, iron, and copper, respectively, while less oxidation-sensitive metals such as Au, Pt, and Ag produce the lowest gas formation (Fig. 10c). The authors suggest that the standard reduction potential (E^0) of these elements influences the volume of gas formed. In the PLAL system, the elements with negative E^0 values readily react with water vapor to form oxides and molecular hydrogen as a side product.[86] The formation of more gas bubbles for these types of elements results in a lower ablation yield due to the shielding of the incoming laser beam (Fig. 10d).[86] Meanwhile, noble metals such as Au and Pt are less prone to oxidation, thus, the gasses formed during the PLAL of these elements are associated with the laser-induced breakdown of the liquid molecules.[86,155,156]

Unlike cavitation bubbles, which can be spatially and temporally located, thus allowing the implementation of bypassing strategies, persistent microbubbles exhibit an unpredictable evolution that limits their bypass. Consequently, liquid flow strategies such as a high flow rate and good laminar flow represent the best approach to remove the detached persistent bubbles. Controlling the liquid flow by the chamber design becomes a fundamental factor for PLAL upscaling since turbulences would extend the retention time of these shielding bubbles inside the chamber, resulting in a reduction of the process efficiency.

4.6. Knowing the effect of target morphology

The morphology of the target influences PLAL productivity due to the different shapes, lifetimes, and dynamics of the produced bubbles. These bubble dynamics influence NP formation. Kohsakowski *et al.* (2016)[100] studied 3 different target geometries: wire tip, clamped wire, and bulk target, in relation

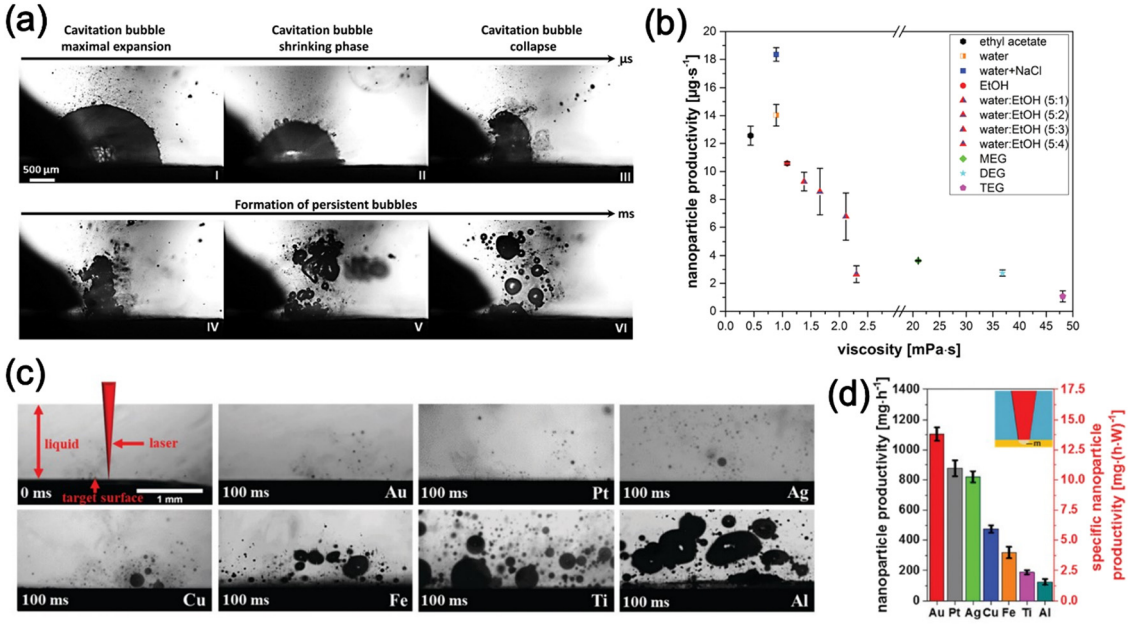

Fig. 10 The influence of persistent microbubbles on the productivity. (a) The formation of persistent microbubbles and (b) the influence of liquid viscosity on the productivity of Au ablation in the respective liquids. Adapted from ref. 145 with permission from the PCCP Owner Societies, copyright 2017. (c) The formation of persistent microbubbles in the ablation of different elements and (d) NPs productivity and power specific productivity for different elements. Adapted from ref. 86 with permission from the PCCP Owner Societies, copyright 2019.

to their bubble formation and dynamics for a single pulse experiment (Fig. 11). Ablation at the tip of the wire results in a 23% shorter bubble lifetime compared to the ablation in a bulk target, due to the springboard movement, which allows a larger displacement of the bubble, as shown in Fig. 11b. This springboard movement also provides a larger displacement of the bubble rebound from the target, compared to the clamped wire and the bulk target (Fig. 11a and c, respectively), which showed a longer duration of the bubble rebound attachment to the target. Multi-pulse experiments were also performed to evaluate PLAL productivity for these three geometries. Wire-type targets (clamped wire and wire tip) showed a productivity increase of up to 2.5 times higher compared to the bulk target. The productivity increase is associated with the elasticity of the wires, which can provide better bubble movement. Nevertheless, the spring-like movement of the wire tip target does not increase the productivity compared to the clamped wire target, due to the limitation in the ablation set-up where the incident laser is shielded by the bubbles rising upward. The authors suggest that the productivity could be improved if the liquid flow is perpendicular to the target which helps to transport the bubbles away from the ablation area.

In a different study, the influence of the wire diameter on PLAL productivity was evaluated for a silver wire target ablated by a 10 ns laser. The highest ablation efficiency is found for a wire diameter of 750 µm, resulting in a 2 times higher ablation rate than the wire diameter of 1500 µm.[89] Based on these two reports, a wire target is an interesting target geometry to increase PLAL productivity due to the changes in bubble dynamics. The modification of the silver target geometry (wire or bulk) does not influence the NP size distribution.[89] Nevertheless, a wire target requires precise laser beam positioning to get the correct focalization of the beam on the wire surface, and not all materials are available as wire shapes. Hence, conventional targets in a form of a bulk plate or a compressed powder pellet are still chosen over the wire shape for easier beam positioning and availability.

Not only the shape but also the texture[157] of the target's surface affect how the laser beam interacts with the target. Nadarajah *et al.* (2020)[158] studied the correlation between the change of surface microstructure during picosecond PLAL with the productivity of some metals and alloys, such as Fe, Au, Ag, and their binary alloys. In the study, the formation of laser-induced periodic surface structures (LIPSS) was observed on the ablated surface of Au and Fe targets and their binary alloys, while Ag does not show the formation of LIPSS (Fig. 12a). Regarding the productivity, it is suggested that the formation of LIPSS on the surface of some alloys affects the reflectivity, as measured for the reflectivity of $Ag_{50}Au_{50}$ without LIPSS formation that is 20% lower compared to the surface with LIPSS.[158] Since LIPSS stem from the linear polarization of the laser, using a quarter wave plate to convert the linear polarization to circular polarization was found to reduce LIPSS formation and increase the productivity of the metal alloys tested (Fig. 12b). Nevertheless, LIPSS is a material specific and fluence-specific phenomenon, and the correlation of LIPSS to the PLAL productivity is still newly explored, hence, further studies are required.

The compactness (degree of porosity) of the target should also be considered to avoid biased results of the productivity due to the removal of large parts of the target not contributing to NP formation. Schmitz *et al.* (2016)[48] compared the gravimetrical and optical (extinction) techniques to measure the

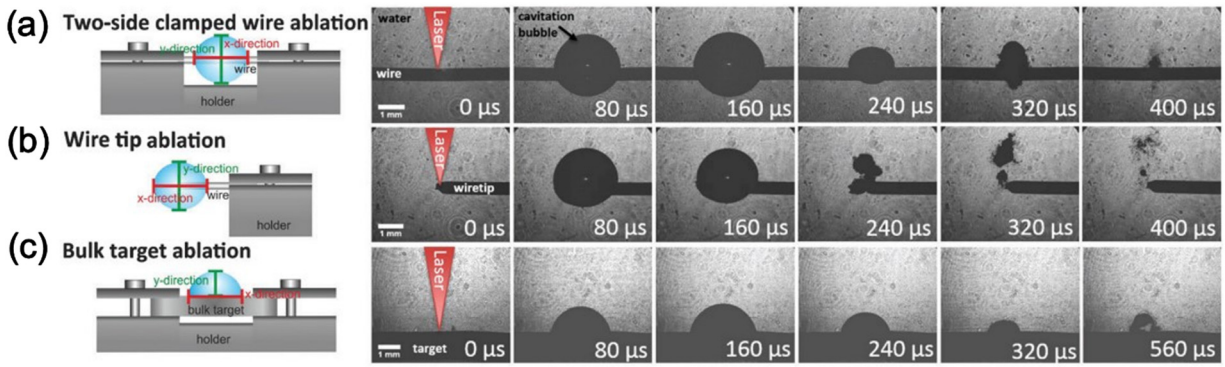

Fig. 11 Bubble morphology depending on the target geometry of (a) wire target clamped on both ends, (b) wire target clamped on one end, and (c) bulk target. Adapted from ref. 100 with permission from the PCCP Owner Societies, copyright 2016.

productivity of targets with different porosity, namely micro-powder-pressed targets (69, 76, and 87% density), a nano-powder-pressed target (99% density), and a bulk target (100% density).[48] The micro-powder-pressed targets showed the highest productivity in the gravimetrical approach compared to the nanopowder-pressed and bulk targets. The absorption measurements indicated that the absorbance values remained fairly consistent across the three samples. However, the apparent contradiction can be attributed to the formation of larger particles in the micro- and millimeter range from the low-density targets, which led to higher productivity values in gravimetric measurements. The absorbance values, on the other hand, only represent smaller particles, which were stable in the colloid during the measurement. The bigger particles already settled at the bottom in less than one minute, thus, did not increase the concentration of the colloid. Hence, it is important to use densely packed pressed powder or bulk targets to avoid biased result especially when PLAL productivity is characterized by the gravimetrical approach.

There is a significant correlation between the target morphology and the productivity of the PLAL system due to its influence on the bubble formation and the laser interaction with the target and liquid. Cylindrical target such as wire is shown to improve the productivity due to the spring-like movement which reduces the bubble lifetime, but the small area makes it difficult to align the beam. Moreover, the curved shape changes the focusing condition within the ablated area, thus resulting in uneven fluences. The plate and sheet types are the most commonly used targets for ablation due to their flat surface and accessibility from the manufacturing company. Employing the flat target is thus recommended. Compact targets such as pressed powder with high density and low porosity, or bulk metal and alloy targets should be used in order to avoid the removal of larger particles.

4.7. Optimizing the ablation chamber design

The simplest ablation chamber design in PLAL is a glass beaker or a cuvette where the target is placed either laying or standing depending on the direction of the incoming beam (Fig. 13a). This setup is sufficient for the production of NPs in a small batch, but for larger production, the employment of these chambers is no longer feasible. Due to the limited volume of the chamber, the colloid becomes concentrated rapidly, which hinders the incoming laser beam to reach the target. In addition, the NPs and persistent bubbles that are formed scatter the incoming laser beam since there is no liquid flow to remove them.[159] Hence, different chamber designs have been proposed to improve the

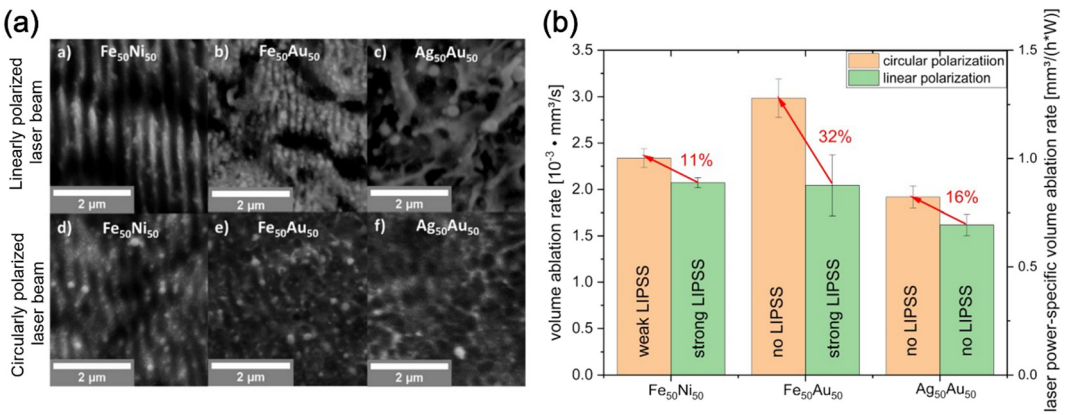

Fig. 12 The influence of laser polarization on the laser-induced periodic surface structures (LIPSS) formation for picosecond PLAL of different targets. (a) SEM images and (b) productivity increase with different laser polarization. Adapted from ref. 158 with permission from The Optical Society, copyright 2020.

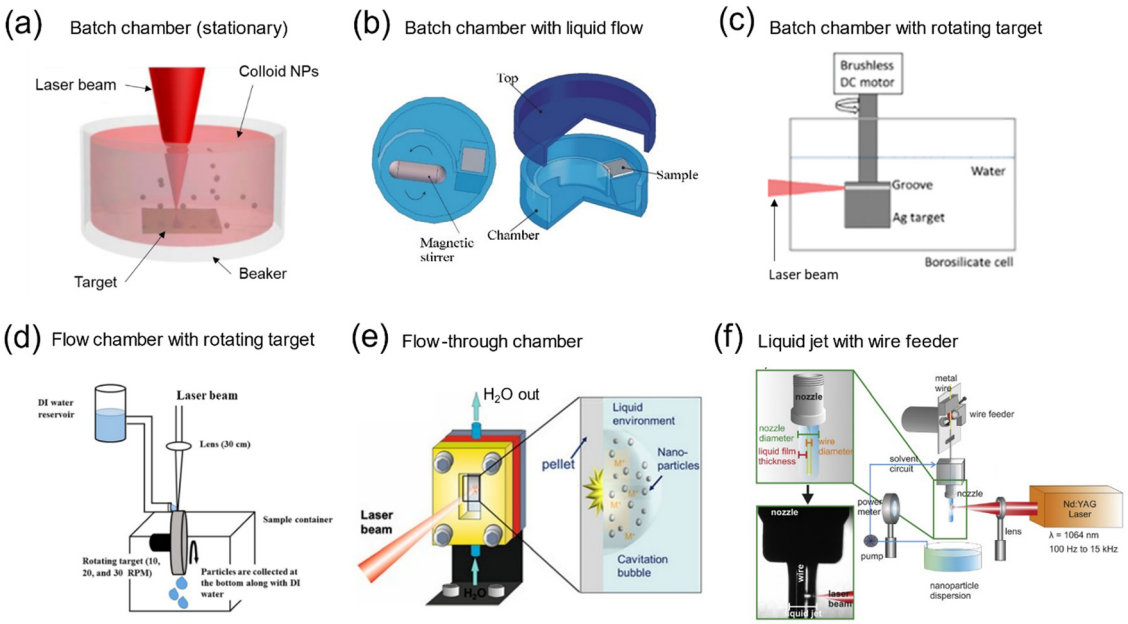

Fig. 13 Type of ablation chambers in the LAL: (a) stationary batch chamber, (b) batch chamber with the liquid flow (reproduced from ref. 114 with permission of AIP Publishing, copyright 2007), (c) batch chamber with rotating target (adapted from ref. 87 with permission from the PCCP Owner Societies, copyright 2016), (d) flow chamber with a rotating target (adapted from ref. 160 with permission from SNCSC, copyright 2017), (e) flow-through chamber (adapted from ref. 161 with permission from Elsevier, copyright 2017), (f) liquid jet with wire feeder (reproduced from ref. 88 with permission from Elsevier, copyright 2017).

PLAL production rate. Barcikowski *et al.* (2007)[114] presented a type of batch chamber with a magnetic stirrer to make the liquid flow inside the chamber (Fig. 13b). The liquid flow inside the chamber is aimed to induce target cooling during ablation and displace the generated NPs away from the target to reduce laser shielding. With this setup, the productivity of femtosecond laser ablation is increased from 0.79 ± 0.36 mg h^{-1} (stationary) to 3.0 ± 0.4 mg h^{-1} (liquid flow). The authors also compared ablation using a picosecond laser with higher pulse energy and repetition rate, resulting in an NP production rate of 31.0 ± 0.4 mg h^{-1} (liquid flow).

A different approach includes the liquid flow within the chamber produced by the rotation of the cylindrical target attached to a brushless motor, as shown in Fig. 13c.[87] At the same time, the rotating target drives away the generated NPs from the vicinity of the target and increases the inter-pulse distance reducing cavitation bubble shielding.[87] The influence of the rotation speed on the ablation rate was evaluated by the colloidal optical extinction approach. The highest PLAL productivity was found at the lowest rotation speed (300 rpm), decreasing with the increasing rotation speed. Based on the flow simulation results as shown in Fig. 14, increasing the rotation speed leads to the formation of unsteady flows and vortices in front of the target's surface, which traps the bubbles produced during PLAL increasing laser shielding.[87] A similar result, reporting lower ablation efficiency with the increasing speed of the rotating target was reported for the ablation of NiTi in water.[160] In this case, the target rotated while the liquid was poured on the ablation spot instead of rotating the target immersed in the liquid, as shown in Fig. 13d. The authors suggest that the high ablation rate with lower rotation speeds is due to close pulse proximity and overlapping effects, which might improve laser absorption of the next pulse.[160]

The next evolution in chamber design is a flow-through chamber that allows PLAL with a continuous feed of fresh liquid and collection of the generated colloid[161] (Fig. 13e). The liquid is pumped through the chamber where ablation takes place, and the generated NPs are carried out of the ablation chamber so that laser shielding is avoided. An optimum liquid flow rate is achieved when the generated NPs are completely removed from the ablation area, confirmed by monitoring the productivity with increasing flow rates.[53] An advantage of this chamber is the capacity to extend PLAL without a colloid concentration saturation and is only limited by the target drilling which allows processing times of several hours even for thin (1 mm) targets.[52]

Alternative flow chamber designs include a nozzle and a wire feeder (Fig. 13f) to reduce the liquid layer thickness and achieve long-term ablation by continuously feeding the target material into the system.[88] This novel system avoids the batch chamber's main limitation for PLAL large productivity, which is the need to replace the liquid frequentlz as NPs concentration reaches a saturation value that does not allow the laser beam to reach the target. The flow chamber is more efficient than the batch chamber, but focus readjustment is still needed due to the depletion of the target's thickness. Meanwhile, a wire target feeder in a liquid jet setup provides the option to feed continuously the target material while keeping the advantages of a continuous liquid flow (Fig. 13f). Prospectively, this setup is proposed to be more efficient, as there is no need to stop the ablation to change

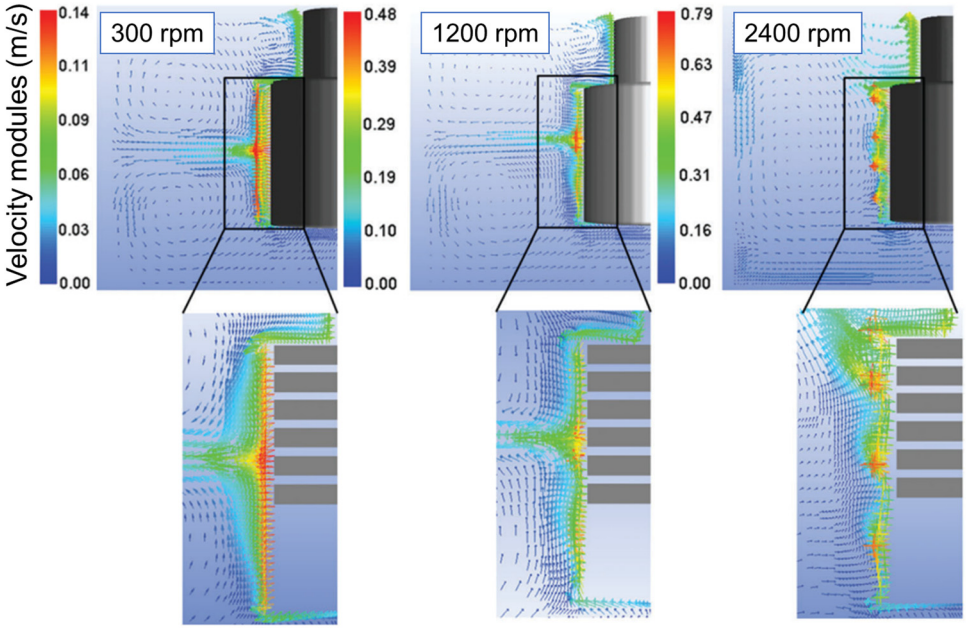

Fig. 14 Numerical simulation of the liquid dynamics inside the rotating target chamber at different rotating speeds. The bottom panels show the magnification of the region on the target surface and the grey rectangles represent the groves produced by the laser. Adapted from ref. 87 with permission from the PCCP Owner Societies, copyright 2016.

the target and/or the liquid. Nevertheless, due to the small wire size, the beam alignment takes longer and represents a major challenge compared to the flow chamber bulk targets. In addition, the stability of the wire feed system represents a challenge for long-term ablation, as well as control of the incident laser fluence. The advantages described and the easier handling and alignment turn the flow through chamber design into the current standard for PLAL upscaling.

Even though the wire feed setup presents some challenges, it highlights another approach to increase PLAL production: liquid layer reduction. It has been reported that decreasing the liquid layer thickness from 8 to 2.5 mm improves the PLAL productivity of an α-Al_2O_3 pressed target from 172 to 592 mg h^{-1}.[53] The authors suggest that absorption and scattering of the laser energy by the generated NPs reduce the laser energy deposition on the target's surface. In a different work, it was reported an optimum liquid layer thickness of 1.2 mm to get the highest yield of Ge NPs in water, based on absorbance characterization.[162] The liquid layer thickness effect was also evaluated in a flow chamber with a silver wire target. Different nozzles were employed to create various liquid layer thicknesses. The optimum productivity was obtained for a liquid layer thickness of 0.5 mm (243 mg h^{-1}). For a liquid layer thickness below 0.3 mm, the ablation showed low reproducibility, which is suggested to stem from partial ablation in air and liquid ejection.

Following this idea, Monsa *et al.* (2020)[91] proposed a strategy to increase NP productivity by focusing the beam at the meniscus interface of a tilted target, as shown in Fig. 15a. An order of magnitude larger concentration of the Pd, Cu, and Ag colloids in ethanol was reported.[91] The comparison of the colloids generated after 5 minute ablation at the meniscus interface and 4 mm liquid layer thickness is shown in Fig. 15b. It should be noted, however, that the optimum liquid layer thickness depends on the material and the experimental set-up (laser parameters, ablation chamber, target and liquid properties, and focusing method) since higher intensities can lead to vaporization of a thicker liquid layer and strong scattering of the beam.

The flow chamber reduced the liquid layer by a closed chamber design and irradiation of the target through a glass window. In this case, extra precautions must be taken to avoid damage to the window glass. The high-temperature plasma plume, shockwave, cavitation bubble, and nanoparticle ejection can cause damage to the window glass if the distance between the target and the window glass is too narrow. It is usually recommended to have a distance of at least 3 mm to avoid damaging the window; naturally, this value depends on other parameters, such as pulse energy, pulse width, and focusing condition. For the ablation without a window (open chamber), the liquid layer thickness could be much lower, but keeping the linear flow represents a major challenge if a large liquid flow rate is employed. These turbulences in the liquid surface affect the laser focusing on the target. Removing the liquid flow allows a stable and thinner liquid layer, however, the effect of the NP shielding due to the rapidly growing colloid concentration represents a larger limitation for PLAL upscaling.

Many ablation chamber designs are proposed to increase the productivity and improve the efficiency of the PLAL process, nevertheless, the discussion related to the fluid dynamics inside the chamber is limited. As the design of the chamber strongly influences the liquid flow, an ineffective chamber produces fluid turbulences which increases the retention time of the NPs inside the chamber, giving rise to the NPs shielding effect of the incoming laser beam. Producing ablation

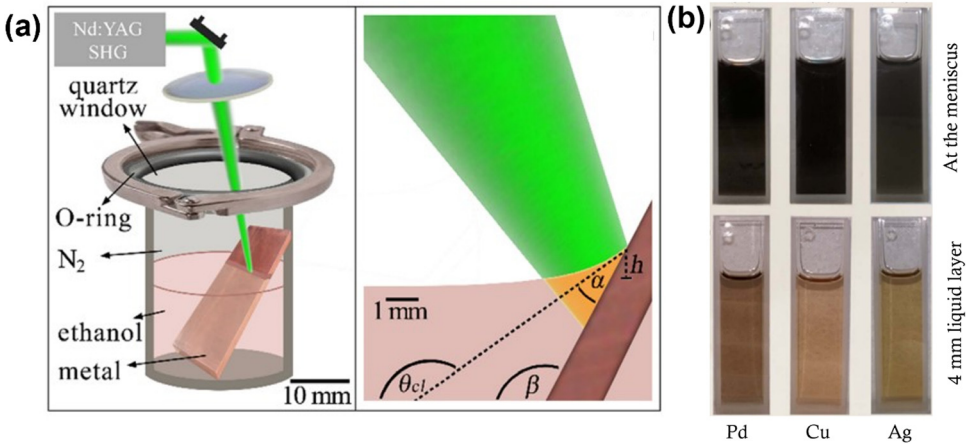

Fig. 15 Proposed strategy to increase productivity by ablating at the meniscus interface of the liquid layer and tilted target. (a) Schematic illustration of the experimental set-up and the enlarged view of the beam at the interface of liquid-target, (b) the colloidal dispersions of Pd, Cu, and Ag NPs produced at the meniscus interface (top) and liquid thickness of 4 mm (bottom). The production of NPs at the meniscus resulted in an order of magnitude higher concentrations compared to the ablation at 4 mm liquid layer thickness. Adapted from ref. 91 with permission from IOP Publishing Ltd, copyright 2020.

chambers with a laminar flow is needed to increase ablation efficiency and the productivity. To produce a laminar flow, a fluid dynamic simulation of the newly designed chamber should be done prior to the production step, to analyze the formation of turbulences and vortices. Studying different liquid viscosities and the influence of species and effects generated by the PLAL process, including the persistent gas, nanoparticles, heat transfer, and the collapse of the cavitation bubbles, are some further stages that can be done in this regard. In summary, the design of an ablation chamber should be accompanied by an engineering approach of fluid mechanical design, which addresses the shortcomings of the inefficient chamber in order to produce laminar flow with minimum turbulence and vortices.

4.8. Continuous production, automatization, remote monitoring, and control of the ablation process

One of the advantages of the PLAL process to produce NPs is the option to perform continuous production. Unlike the wet chemical synthesis methods where the NPs production is commonly done in batches using a certain recipe with tight control over reactants amount and synthesis conditions, continuous production in PLAL can be performed simply by using a flow chamber, either with or without the recirculation of liquid (loop) as shown in ref. 163 for the ablation of a gold target using a nanosecond laser. The continuous production of NPs in the industry is critical to reducing the cost, yet scaling up the batches of chemical synthesis procedure is not as easy as multiplying the amount of the reagents and increasing the reactor's volume. Various parameters such as the reactants concentration, amount of catalyst and stabilizer, heating temperature, stirring speed, and the duration of each process should be optimized accordingly.[164] Moreover, the properties of NPs could possibly change during the scaling up, as the nanoscale control is difficult at larger reactants quantity.[164]

To ensure both safety and economic efficiency, it would be ideal for the implementation of PLAL in the industry to include an automated system for controlling and remotely monitoring the ablation process.[165,166] As the PLAL process only requires the operator for the first setup and periodical monitoring of the status,[166] the required automatization and remote controlling include maintaining the optimum working distance,[165,167] regulating the liquid flow,[166,168] and controlling the laser.[166]

In terms of the automatic control of the working distance, the utilization of acoustic emission as the input data to control the working distance has been proposed. The acoustic emission is considered more practical than the gravimetric approach where the target has to be periodically removed, and it is also applicable in a wide range of material composition, colloid concentration, particle size, and shape,[165] which prove its advantage compared to the extinction approach discussed in Section 3. Definition and measurement of nanoparticle productivity. A prior study by Zhu *et al.* (2001)[169] proved the correlation between material productivity in PLAL and the produced intensity of the audible acoustic waves (sounds) measured by a wideband microphone. Afterward, the following studies to use acoustic emission not only to monitor the production rate of a PLAL process but also to control the system were performed by another group.[165,167] The system uses a piezoelectric sensor to record the acoustic emission waveforms during the PLAL process and the data is forwarded to a Field Programmable Gate Array (FPGA)-based system coupled by Discrete Wavelet Transform (DWT), which is able to perform an online, real-time processing of the acoustic emission while reducing the noise and accelerating the processing time (Fig. 16a). To find and maintain the ideal working distance, an iterative search algorithm is employed by finding the maximum acoustic wave energy (amplitude) at various working distances. The system is thus connected to a stepper motor, which can automatically position the ablation chamber based on the received acoustic emission data.[165,167] Based on the comparative study with the UV-Vis spectra, this system shows similar results as shown in Fig. 16b,[165,167] offering a reliable option for the automatic adjustment of the working distance.

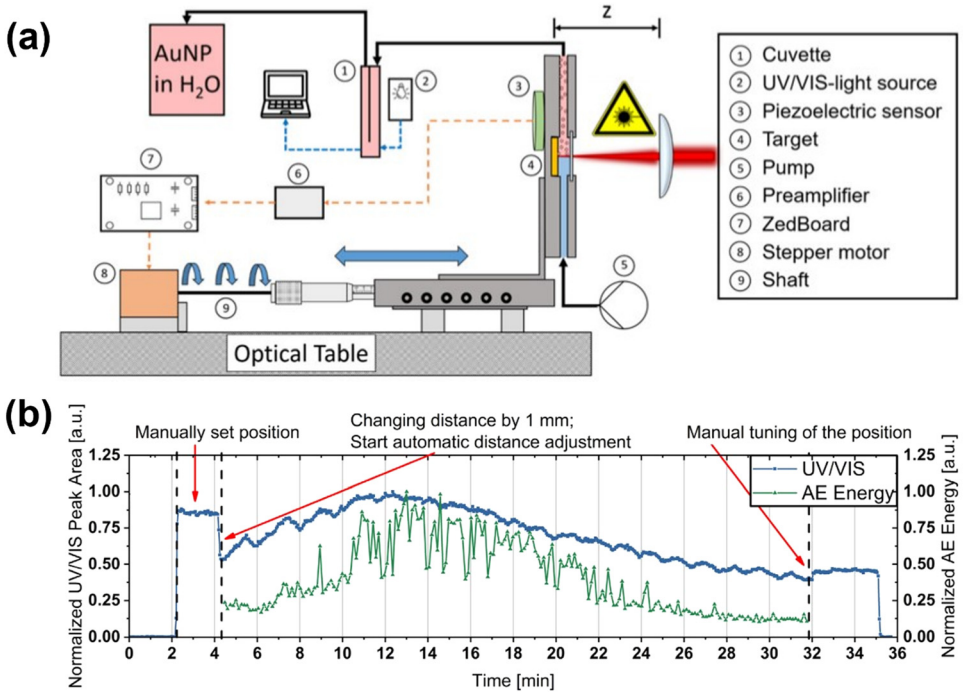

Fig. 16 Real-time monitoring and automatic control of the working distance in the PLAL system, where (a) shows the experimental set-up and (b) shows the comparison between the acoustic emission (AE) signal and UV-Vis spectra over time. Adapted from ref. 167 with permission from Elsevier, copyright 2019.

The automatization of the liquid flow is proposed by Freeland *et al.* (2020)[168] in order to produce NP colloids with a high concentration using a semi-batch recirculatory flow system. The common production step of NP colloids with high concentration requires a separate post-processing step, such as magnetic decantation, centrifugation, destabilization, or vaporization of the liquid, which is time-consuming. By recirculating the liquid flow, the concentration of NP colloid can be increased until the desired value. The liquid flow control is operated through a LabVIEW program which is connected to an automatic valve and peristaltic pump.[168] Unfortunately, there is no discussion on how the automatization of liquid flow using the automatic valve is done.

Complete remote monitoring and controlling of a PLAL system were built using the combination of a LabVIEW program and a TeamViewer program (Fig. 17a).[166] The LabVIEW program is used to control the instruments by connecting them to the on-site PC using a serial connector and several devices are controlled by the PC, namely the laser, the pump, the interlock webcam, the camera, and the XY-stage (Fig. 17b). Meanwhile, the TeamViewer program is used to remotely access the on-site PC, either from a smartphone or an off-site PC (Fig. 17b). With this online, remotely controlled setup, the PLAL system can be accessed from any place with an internet connection having bandwidth larger than 1–0.1 Mbytes s^{-1},[166] and the response time for shutting off the laser

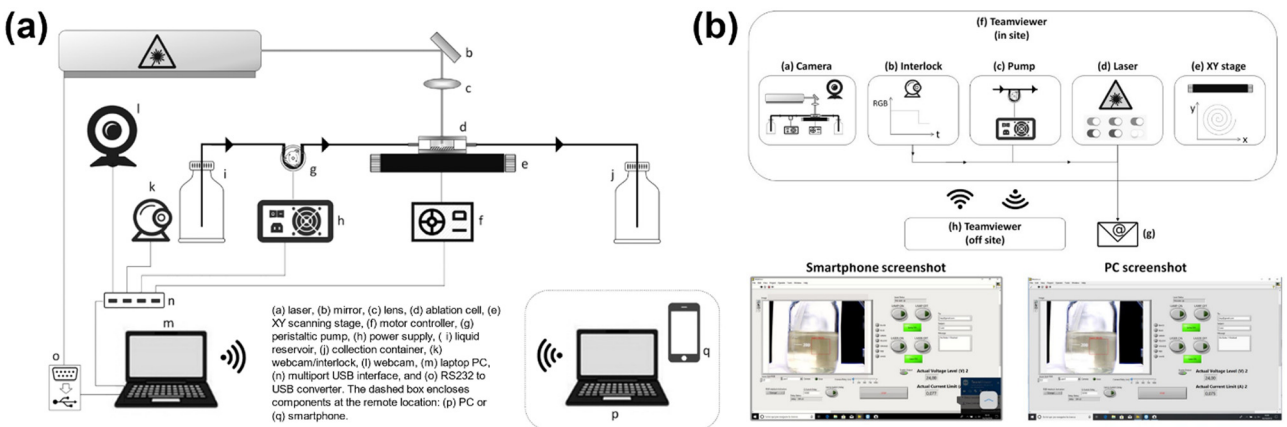

Fig. 17 Remote monitoring and controlling system. (a) Schematic representation of the system configuration, (b) controlled devices with in-site PC and the screenshot of off-site controlling devices. Adapted from ref. 166 with permission from AIP Publishing, copyright 2019.

is of 10^{-3} s.[166] In case of the automatization, the system offers an automatic shutdown when the colloid concentration, measured by the interlock webcam coupled with color analysis software, reaches the desired threshold value. The interlock webcam is also used to gauge the liquid amount in the bottle, thus preventing liquid spillover and running out of liquid.[166] The set-up presents a solution to the industrial needs where off-site controlling is required, for example in the ablation process of dangerous substances, such as radioactive materials. In addition to that, it provides a more efficient and practical way to control the PLAL process from anywhere, while the automatization allows us to produce colloidal NPs with certain concentrations and prevent undesired lab accidents, even without constant human supervision.

The development of automatization, remote monitoring, and off-site controlling of the PLAL process is necessary to open the pathway of PLAL usage in the industry. Automatization offers a faster task execution based on feedback systems, which results in a more efficient and economical way compared to the manual adjustment by labor workers. It also reduces the chance of human error during the process, thus avoiding the chance of laboratory and industrial accidents. The automatization to produce certain colloid concentrations and automatically stop the laser system means that the expenses for labor workers could be minimized. The remote monitoring and off-site controlling provide us with the ability to control on-site experiments from anywhere, which means that the operator does not need to be continuously present nearby the PLAL system. The shown configuration in this subchapter is still limited to a laboratory experiment with a small production batch, but the system is potentially applicable for the production of large batches of NP colloids such as in tens or hundreds of liters. Coupled with an injectable manufacturing process, the use of a high-power laser, a fast scanner, a large and efficient ablation chamber, a continuous liquid flow, automatization, and a remotely controlled system, the production of colloidal nanoparticles for industrial application could surely be achieved.

5. Conclusion and outlook

We have conducted a thorough re-examination of the factors that influence the productivity of PLAL. Based on the discussion of the laser and target properties, it should be noted that several parameters such as laser fluence and wavelength, the target properties, and the focal length, among others, should be taken into account in each experiment to comprehensively evaluate the productivity of PLAL. Although it appears that productivity is strongly linked to the material and architecture of the ablation system, the PLAL method still holds high potential to be used widely in industry. The advantages offered by PLAL over the chemical synthesis method lies in the possibility to produce various type of nanoparticles from bulk materials in a straightforward manner as it only requires a laser, a scanner, a chamber, a liquid, and a target. To produce a different type of nanoparticle composition, one can simply change the target, which varies from metal, ceramics, and alloy to organic compounds. Meanwhile, in the conventional synthesis method, each type of desired nanoparticles requires new ingredients, reagents, catalysts, and optimization of each physical treatment step (stirring, heating, exposure to certain gas). The challenge with the low production rate can be overcome by other means which are not directly related to the material properties or laser parameters, such as using a high scanning speed, a chamber with laminar flow and small liquid layer thickness, and the use of additional optical elements to change the beam profile. Besides, the gram-per-hour production rate of NPs has been achieved for different materials by increasing the interpulse distance and bypassing the cavitation bubble.[52–54,74,170]

As a general guideline, higher productivities of PLAL can be obtained by the utilization of high power and repetition rate picosecond laser sources, which can mitigate nonlinear interactions, in conjunction with a fast-scanning strategy to circumvent the cavitation bubble spatially. In addition to the laminar liquid flow with a reduced layer, when feasible, it is advised to use low-viscosity liquid to prevent the shielding of nanoparticles and eliminate persistent bubbles.

As we have shown, considerable efforts have been devoted to enhancing productivity over the course of this century, resulting in remarkable advancements of up to three orders of magnitude, leading to outputs in the range of grams per hour. Nevertheless, certain unresolved issues remain that require attention to facilitate further improvements.

- The automatization of the PLAL process. Automated processes perform tasks much faster than humans and the use of feedback systems allows for adjustments to be made on the fly of the fabrication. By removing human intervention from certain tasks, such as the focalization of the beam over the target, the refill of the liquid, and the cleaning of the components, variations due to human error can be minimized. Furthermore, this decrease in the labor-intensive nature of PLAL can save time in situations where production would otherwise need to be halted and, as a result, potentially reduced. Although some preliminary studies have been conducted on monitoring and managing off-site fabrication,[166] greater levels of automation will be necessary to enable the broader commercialization of this technology.
- Enhance productivity across various pulse duration regimes. Laser pulse width impacts the mechanism of synthesis of the nanomaterial at multiple stages, as evidenced by large-scale atomistic simulation,[68] thereby influencing the nanomaterials properties such as the morphology,[171] the composition,[38] the atomic redistribution of metal domains,[172] the oxidation and aging effects,[173] the shape,[174] and the crystalline size domains[175] among others. Using pulse widths in the femtosecond and nanosecond range represents an approach to synthesizing different nanomaterial properties without additional post-production steps, which is interesting for industrial setup. As an example, lattice heating and prolonged plasma exposure from the nanosecond pulses can stimulate the phase transition of the NPs, such as the reversible transformation between nanodiamond and carbon-onion structure,[176] the restructuring

and surface decoration of RuO_2 nanoparticles to RuO_2@Ru/RuO_2,[177] and the formation of carbon-based quantum dots with either graphene or amorphous structure.[178,179] The use of a thermosetting polymer solution as the ablation liquid for nanosecond PLAL can promote different core–shell structures.[38,180,181] In addition, femtosecond lasers allow to obtain the atomic redistribution in bimetallic Au–Pd nanorods[172] and reshape gold nanorods with ultranarrow surface plasmon resonances.[174] Consequently, to achieve precise control of PLAL nanomaterials, it is essential to improve productivity across different pulse width regimes and not settle for high production solely with picosecond pulses. Furthermore, it should be noted that extreme pulse durations in the attosecond range have yet to be utilized for generating nanoparticles in PLAL.

• The utilization of temporal pulse tailoring strategies. The ability to manipulate the temporal profile of the laser pulse enables the energy rate to be tailored to the specific material reaction. Although various techniques have been used for temporal beam manipulation, such as double-pulse laser irradiation,[147,182,183] or irradiation with a burst of pulses,[184] there is still room for improvement to maximize productivity. Some of these techniques require further study, while others can be introduced for the first time in PLAL, such as the conformation of the temporal pulse envelope of ultrashort pulses.

• To use fluid mechanics simulations (CFD) to optimize the nanomaterial ablation. Although different strategies related to fluid dynamics have been developed to increase production rate, as explained in the variations of the ablation chamber (4.7. Optimizing the ablation chamber design), there is still room for improvement. In this direction, CFD simulations can help to optimize not only the chamber geometry but also the control of turbulence, bubble removal, reduction of areas of nanoparticle accumulation, and selection of suitable liquids based on viscosity, density, and refractive index, among others.

• The implementation of smart beam delivery optical systems for controlling pulse the spatial distribution of the energy over a target. Galvanometric scanners and polygonal wheels are commonly used for beam delivery in PLAL. However, the focal length of these setups is typically fixed, and this determines key parameters, such as the numerical aperture, the fluence, and the spot size that constrains the flexibility of the ablation processes. Therefore, some flexibility in the beam delivery must be considered for further improvements in productivity. Our recommendation is to integrate advanced smart beam delivery devices, such as the SSTF system that mitigates non-linearities, into high-speed scanners. Additionally, dynamic (spatial light modulators) or static (diffractive optical elements or freeform optics) beam-shaping elements can be utilized. Given that the current high-power laser used in PLAL exceeds the required optimum energy for laser ablation by several orders of magnitude, parallel processing presents an efficient alternative to reduce processing time.[185] Furthermore, different spatial profiles at the focus can be designed[186] to study how they affect the laser-matter interaction and influence the ablated mass. Finally, it is crucial for the PLAL scientific community to keep abreast of the research that emerged in the last few years regarding the use of smart beam delivery systems for focusing through turbid media,[187] as some of the devices developed for other disciplines may be adapted for its use in PLAL.

• Artificial intelligence (AI) has the potential to enhance productivity by optimizing the various parameters involved in the PLAL process. Through the analysis of vast amounts of data on target material properties, laser parameters, and liquid media, AI algorithms can identify optimal conditions for nanoparticle synthesis, resulting in a more efficient, reproducible, and productive PLAL process. Moreover, this advanced knowledge of the optimal PLAL conditions can facilitate the rapid scaling-up of production by minimizing trial-and-error experimentation and will help to generate large-scale production to meet the market demands.

• Although laser power and repetition rates have been increasing, scanner technology remains a bottleneck in achieving high ablation rates. Therefore, there is a need for improvements in the current laser and scanning technology. All the improvements in the laser technology or the high-speed scanning systems will have a direct impact on PLAL productivity.

To conclude, as the global population continues to increase alongside its corresponding demands, the imperative for more efficient methods to synthesize nanomaterials will undoubtedly intensify. In this regard, PLAL has emerged as a promising approach with a myriad of applications, supported by a large community of researchers who are actively pursuing the development of eco-friendly technology. Continuously striving to enhance PLAL productivity represents a crucial endeavor, as it has the potential to make the green fabrication of nanomaterials more affordable and accessible to a wider range of consumers, researchers, and industries. Moreover, such advancements will undoubtedly broaden the horizons of its potential applications.

Author contributions

Writing – original draft I. Y. K., C. D.-B., G. M.-V; writing – review & editing I. Y. K, C. D.-B., G. M.-V, B. G; visualization I. Y. K, C. D.-B; supervision C. D.-B, B. G.; project administration C. D.-B, B. G.; funding acquisition C. D.-B, B. G.

Conflicts of interest

There are no conflicts to declare.

Acknowledgements

The authors acknowledge funding by the Deutsche Forschungsgemeinschaft (DFG, German Research Foundation), grant numbers GO 2566/10-1 and GO 2566/14-1, and the European Union's Horizon 2020 research and innovation program under the grant agreement No. 952068 (project LESGO).

References

1 L. Kool, F. Dekker, A. Bunschoten, G. J. Smales, B. R. Pauw, A. H. Velders and V. Saggiomo, Gold and silver dichroic nanocomposite in the quest for 3D printing the Lycurgus cup, *Beilstein J. Nanotechnol.*, 2020, **11**, 16–23, DOI: 10.3762/bjnano.11.2.

2 I. Freestone, N. Meeks, M. Sax and C. Higgitt, The Lycurgus Cup—A Roman nanotechnology, *Gold Bull.*, 2007, **40**(4), 270–277, DOI: 10.1007/BF03215599.

3 A. K. Gupta and M. Gupta, Synthesis and surface engineering of iron oxide nanoparticles for biomedical applications, *Biomaterials*, 2005, **26**(18), 3995–4021, DOI: 10.1016/j.biomaterials.2004.10.012.

4 Q. A. Pankhurst, J. Connolly, S. K. Jones and J. Dobson, Applications of magnetic nanoparticles in biomedicine, *J. Phys. D: Appl. Phys.*, 2003, **36**(13), R167–R181, DOI: 10.1088/0022-3727/36/13/201.

5 D. A. Giljohann, D. S. Seferos, W. L. Daniel, M. D. Massich, P. C. Patel and C. A. Mirkin, Gold nanoparticles for biology and medicine, *Angew. Chem., Int. Ed.*, 2010, **49**(19), 3280–3294, DOI: 10.1002/anie.200904359.

6 R. Pérez-Tanoira, M. Fernández-Arias, C. Potel, R. Carballo-Fernández, S. Pérez-Castro, M. Boutinguiza, M. Górgolas, F. Lusquiños and J. Pou, Silver Nanoparticles Produced by Laser Ablation and Re-Irradiation Are Effective Preventing Peri-Implantitis Multispecies Biofilm Formation, *Int. J. Mol. Sci.*, 2022, **23**(19), 12027, DOI: 10.3390/ijms231912027.

7 Y. Liang, Y. Li, H. Wang, J. Zhou, J. Wang, T. Regier and H. Dai, Co_3O_4 nanocrystals on graphene as a synergistic catalyst for oxygen reduction reaction, *Nat. Mater.*, 2011, **10**(10), 780–786, DOI: 10.1038/nmat3087.

8 Y. Li, H. Wang, L. Xie, Y. Liang, G. Hong and H. Dai, MoS 2 Nanoparticles Grown on Graphene: An Advanced Catalyst for the Hydrogen Evolution Reaction, *J. Am. Chem. Soc.*, 2011, **133**(19), 7296–7299, DOI: 10.1021/ja201269b.

9 Q. Xiang, J. Yu and M. Jaroniec, Synergetic Effect of MoS_2 and Graphene as Cocatalysts for Enhanced Photocatalytic H_2 Production Activity of TiO_2 Nanoparticles, *J. Am. Chem. Soc.*, 2012, **134**(15), 6575–6578, DOI: 10.1021/ja302846n.

10 J. Theerthagiri, K. Karuppasamy, A. Min, D. Govindarajan, M. L. A. Kumari, G. Muthusamy, S. Kheawhom, H. S. Kim and M. Y. Choi, Unraveling the fundamentals of pulsed laser-assisted synthesis of nanomaterials in liquids: applications in energy and the environment, *Appl. Phys. Rev.*, 2022, **9**(4), 041314, DOI: 10.1063/5.0104740.

11 J. Theerthagiri, K. Karuppasamy, S. J. Lee, R. Shwetharani, H. S. Kim, S. K. K. Pasha, M. Ashokkumar and M. Y. Choi, Fundamentals and comprehensive insights on pulsed laser synthesis of advanced materials for diverse photo- and electrocatalytic applications, *Light: Sci. Appl.*, 2022, **11**(1), 250, DOI: 10.1038/s41377-022-00904-7.

12 S. Naik Shreyanka, J. Theerthagiri, S. J. Lee, Y. Yu and M. Y. Choi, Multiscale design of 3D metal–organic frameworks (M−BTC, M: Cu, Co, Ni) via PLAL enabling bifunctional electrocatalysts for robust overall water splitting, *Chem. Eng. J.*, 2022, **446**, 137045, DOI: 10.1016/j.cej.2022.137045.

13 R. Torres-Mendieta, R. Mondragón, V. Puerto-Belda, O. Mendoza-Yero, J. Lancis, J. E. Juliá and G. Mínguez-Vega, Characterization of Tin/Ethylene Glycol Solar Nanofluids Synthesized by Femtosecond Laser Radiation, *ChemPhysChem*, 2017, **18**(9), 1055–1060, DOI: 10.1002/cphc.201601083.

14 M. B. Wilms, N. Pirch and B. Gökce, Manufacturing oxide-dispersion-strengthened steels using the advanced directed energy deposition process of high-speed laser cladding, *Prog. Addit. Manuf.*, 2022, 0123456789, DOI: 10.1007/s40964-022-00319-1.

15 C. Doñate-Buendía, D. Gu, M. Schmidt, S. Barcikowski, A. M. Korsunsky and B. Gökce, On the selection and design of powder materials for laser additive manufacturing, *Mater. Des.*, 2021, **204**, 109653, DOI: 10.1016/j.matdes.2021.109653.

16 M. J. Hajipour, K. M. Fromm, A. Akbar Ashkarran, D. Jimenez de Aberasturi, I. R. Larramendi, T. Rojo, V. Serpooshan, W. J. Parak and M. Mahmoudi, Antibacterial properties of nanoparticles, *Trends Biotechnol.*, 2012, **30**(10), 499–511, DOI: 10.1016/j.tibtech.2012.06.004.

17 A. Sirelkhatim, S. Mahmud, A. Seeni, N. H. A. Kaus, L. C. Ann, S. K. H. Bakhori, H. Hasan and D. Mohamad, Review on zinc oxide nanoparticles: antibacterial activity and toxicity mechanism, *Nano-Micro Lett.*, 2015, **7**(3), 219–242, DOI: 10.1007/s40820-015-0040-x.

18 A. Jain, L. S. Duvvuri, S. Farah, N. Beyth, A. J. Domb and W. Khan, Antimicrobial Polymers, *Adv. Healthcare Mater.*, 2014, **3**(12), 1969–1985, DOI: 10.1002/adhm.201400418.

19 G. A. Lopez, M. C. Estevez, M. Soler and L. M. Lechuga, Recent advances in nanoplasmonic biosensors: applications and lab-on-a-chip integration, *Nanophotonics*, 2017, **6**(1), 123–136, DOI: 10.1515/nanoph-2016-0101.

20 K. Ai, B. Zhang and L. Lu, Europium-Based Fluorescence Nanoparticle Sensor for Rapid and Ultrasensitive Detection of an Anthrax Biomarker, *Angew. Chemie*, 2009, **121**(2), 310–314, DOI: 10.1002/ange.200804231.

21 Y. Wang, H. Zhang, Y. Zhu, Z. Dai, H. Bao, Y. Wei and W. Cai, Au-NP-Decorated Crystalline FeOCl Nanosheet: Facile Synthesis by Laser Ablation in Liquid and its Exclusive Gas Sensing Response to HCl at Room Temperature, *Adv. Mater. Interfaces*, 2016, **3**(9), 1500801, DOI: 10.1002/admi.201500801.

22 R. Torres-Mendieta, D. Ventura-Espinosa, S. Sabater, J. Lancis, G. Mínguez-Vega and J. A. Mata, In situ decoration of graphene sheets with gold nanoparticles synthetized by pulsed laser ablation in liquids, *Sci. Rep.*, 2016, **6**, 1–9, DOI: 10.1038/srep30478.

23 T. Kim, S. Kang, J. Heo, S. Cho, J. W. Kim, A. Choe, B. Walker, R. Shanker, H. Ko and J. Y. Kim, Nanoparticle-Enhanced Silver-Nanowire Plasmonic Electrodes for High-Performance Organic Optoelectronic Devices, *Adv. Mater.*, 2018, **30**(28), 1800659, DOI: 10.1002/adma.201800659.

24 H. Choi, S. -J. Ko, Y. Choi, P. Joo, T. Kim, B. R. Lee, J. -W. Jung, H. J. Choi, M. Cha, J. -R. Jeong, I. -W. Hwang,

M. H. Song, B. -S. Kim and J. Y. Kim, Versatile surface plasmon resonance of carbon-dot-supported silver nanoparticles in polymer optoelectronic devices, *Nat. Photonics*, 2013, **7**(9), 732–738, DOI: **10.1038/nphoton.2013.181**.

25 N. Baig, I. Kammakakam, W. Falath and I. Kammakakam, Nanomaterials: a review of synthesis methods, properties, recent progress, and challenges, *Mater. Adv.*, 2021, **2**(6), 1821–1871, DOI: **10.1039/D0MA00807A**.

26 M. N. R. Ashfold, F. Claeyssens, G. M. Fuge and S. J. Henley, Pulsed laser ablation and deposition of thin films, *Chem. Soc. Rev.*, 2004, **33**(1), 23, DOI: **10.1039/b207644f**.

27 S. V. Starinskiy, Y. G. Shukhov and A. V. Bulgakov, Dynamics of pulsed laser ablation of gold in vacuum in the regime of nanostructured film synthesis, *Tech. Phys. Lett.*, 2016, **42**(4), 411–414, DOI: **10.1134/S1063785016040258**.

28 Z. Lin, S. Shen, Z. Wang and W. Zhong, Laser ablation in air and its application in catalytic water splitting and Li-ion battery, *iScience*, 2021, **24**(5), 102469, DOI: **10.1016/j.isci.2021.102469**.

29 D. Zhang, Z. Li and K. Sugioka, Laser ablation in liquids for nanomaterial synthesis: diversities of targets and liquids, *JPhys Photonics*, 2021, **3**(4), 1–35, DOI: **10.1088/2515-7647/ac0bfd**.

30 P. P. Patil, D. M. Phase, S. A. Kulkarni, S. V. Ghaisas, S. K. Kulkarni, S. M. Kanetkar, S. B. Ogale and V. G. Bhide, Pulsed-laser – induced reactive quenching at liquid–solid interface: aqueous oxidation of iron, *Phys. Rev. Lett.*, 1987, **58**(3), 238–241, DOI: **10.1103/PhysRevLett.58.238**.

31 A. Fojtik and A. Henglein, Laser ablation of films and suspended particles in a solvent: formation of cluster and colloid solutions, *Berichte der Bunsen-Gesellschaft*, 1993, **97**(2), 252–254.

32 A. Henglein, Physicochemical properties of small metal particles in solution: 'microelectrode' reactions, chemisorption, composite metal particles, and the atom-to-metal transition, *J. Phys. Chem.*, 1993, **97**(21), 5457–5471, DOI: **10.1021/j100123a004**.

33 D. Zhang, B. Gökce and S. Barcikowski, Laser Synthesis and Processing of Colloids: Fundamentals and Applications, *Chem. Rev.*, 2017, **117**(5), 3990–4103, DOI: **10.1021/acs.chemrev.6b00468**.

34 B. Gökce, V. Amendola and S. Barcikowski, Opportunities and Challenges for Laser Synthesis of Colloids, *ChemPhysChem*, 2017, **18**(9), 983–985, DOI: **10.1002/cphc.201700310**.

35 E. Fazio, B. Gökce, A. De Giacomo, M. Meneghetti, G. Compagnini, M. Tommasini, F. Waag, A. Lucotti, C. G. Zanchi, P. M. Ossi, M. Dell'Aglio, L. D'Urso, M. Condorelli, V. Scardaci, F. Biscaglia, L. Litti, M. Gobbo, G. Gallo, M. Santoro, S. Trusso and F. Neri, Nanoparticles Engineering by Pulsed Laser Ablation in Liquids: Concepts and Applications, *Nanomaterials*, 2020, **10**(11), 2317, DOI: **10.3390/nano10112317**.

36 M. Alheshibri, S. Akhtar, A. Al Baroot, K. A. Elsayed, H. S. Al Qahtani and Q. A. A. Drmosh, Template-free single-step preparation of hollow CoO nanospheres using pulsed laser ablation in liquid enviroment, *Arab. J. Chem.*, 2021, **14**(9), 103317, DOI: **10.1016/j.arabjc.2021.103317**.

37 H. S. Desarkar, P. Kumbhakar and A. K. Mitra, One-step synthesis of Zn/ZnO hollow nanoparticles by the laser ablation in liquid technique, *Laser Phys. Lett.*, 2013, **10**(5), 055903, DOI: **10.1088/1612-2011/10/5/055903**.

38 A. Tymoczko, M. Kamp, C. Rehbock, L. Kienle, E. Cattaruzza, S. Barcikowski and V. Amendola, One-step synthesis of Fe–Au core–shell magnetic-plasmonic nanoparticles driven by interface energy minimization, *Nanoscale Horiz.*, 2019, **4**(6), 1326–1332, DOI: **10.1039/c9nh00332k**.

39 I. Y. Khairani, Q. Lin, J. Landers, S. Salamon, C. Doñate-Buendía, E. Karapetrova, H. Wende, G. Zangari and B. Gökce, Solvent Influence on the Magnetization and Phase of Fe–Ni Alloy Nanoparticles Generated by Laser Ablation in Liquids, *Nanomaterials*, 2023, **13**(2), 227, DOI: **10.3390/nano13020227**.

40 Y. Jia, T. -Y. Sun, J. -H. Wang, H. Huang, P. Li, X. -F. Yu and P. K. Chu, Synthesis of hollow rare-earth compound nanoparticles by a universal sacrificial template method, *CrystEngComm*, 2014, **16**(27), 6141–6148, DOI: **10.1039/C4CE00440J**.

41 J. Zeng, J. Huang, W. Lu, X. Wang, B. Wang, S. Zhang and J. Hou, Necklace-like Noble-Metal Hollow Nanoparticle Chains: Synthesis and Tunable Optical Properties, *Adv. Mater.*, 2007, **19**(16), 2172–2176, DOI: **10.1002/adma.200602440**.

42 P. Anastas and N. Eghbali, Green Chemistry: Principles and Practice, *Chem. Soc. Rev.*, 2010, **39**(1), 301–312, DOI: **10.1039/b918763b**.

43 A. N. Arifiadi, K.-T. Kim, I. Y. Khairani, C. B. Park, K. H. Kim and S.-K. Kim, Synthesis and multiferroic properties of high-purity $CoFe_2O_4$–$BiFeO_3$ nanocomposites, *J. Alloys Compd.*, 2021, **867**, 159008, DOI: **10.1016/j.jallcom.2021.159008**.

44 I. Y. Khairani, A. N. Arifiadi, J.-H. Lee, B. Bhoi, S. K. S. Patel and S. Kim, Fabrication, Structure, and Magnetic Properties of Pure-Phase $BiFeO_3$ and $MnFe_2O_4$ Nanoparticles and their Nanocomposites, *J. Magn.*, 2020, **25**(2), 140–149, DOI: **10.4283/JMAG.2020.25.2.140**.

45 I. Kartini, I. Y. Khairani, C. Chotimah, S. Mustofa, S. J. Santosa and L. Z. Wang, The effect of alkaline ratios of NaOH to NH_3 on the formation of nanostructured titania, *Mater. Sci. Forum*, 2017, **886**, 42–47, DOI: **10.4028/www.scientific.net/MSF.886.42**.

46 A. V. Shabalina, V. A. Svetlichnyi and S. A. Kulinich, Green laser ablation-based synthesis of functional nanomaterials for generation, storage, and detection of hydrogen, *Curr. Opin. Green Sustainable Chem.*, 2022, **33**, 100566, DOI: **10.1016/j.cogsc.2021.100566**.

47 V. Amendola, D. Amans, Y. Ishikawa, N. Koshizaki, S. Scirè, G. Compagnini, S. Reichenberger and S. Barcikowski, Room-Temperature Laser Synthesis in Liquid of Oxide, Metal-Oxide Core–Shells, and Doped Oxide Nanoparticles, *Chem. – Eur. J.*, 2020, **26**(42), 9206–9242, DOI: **10.1002/chem.202000686**.

48 T. Schmitz, U. Wiedwald, C. Dubs and B. Gökce, Ultrasmall Yttrium Iron Garnet Nanoparticles with High Coercivity at Low Temperature Synthesized by Laser Ablation and Fragmentation of Pressed Powders, *ChemPhysChem*, 2017, **18**(9), 1125–1132, DOI: **10.1002/cphc.201601183**.

49 A. Chemin, J. Lam, G. Laurens, F. Trichard, V. Motto-Ros, G. Ledoux, V. Jarý, V. Laguta, M. Nikl, C. Dujardin and D. Amans, Doping nanoparticles using pulsed laser ablation in a liquid containing the doping agent, *Nanoscale Adv.*, 2019, **1**(10), 3963–3972, DOI: **10.1039/c9na00223e**.

50 S. Jendrzej, B. Gökce, M. Epple and S. Barcikowski, How Size Determines the Value of Gold: Economic Aspects of Wet Chemical and Laser-Based Metal Colloid Synthesis, *ChemPhysChem*, 2017, **18**(9), 1012–1019, DOI: **10.1002/cphc.201601139**.

51 J. Park, K. An, Y. Hwang, J. Park, H Noh, J Kim, J Park, N Hwang and T Hyeon, Ultra-large-scale syntheses of monodisperse nanocrystals, *Nat. Mater*, 2004, **3**, 891–895, DOI: **10.1038/nmat1251**.

52 R. Streubel, G. Bendt and B. Gökce, Pilot-scale synthesis of metal nanoparticles by high-speed pulsed laser ablation in liquids, *Nanotechnology*, 2016, **27**(20), 205602, DOI: **10.1088/0957-4484/27/20/205602**.

53 C. L. Sajti, R. Sattari, B. N. Chichkov and S. Barcikowski, Gram Scale Synthesis of Pure Ceramic Nanoparticles by Laser Ablation in Liquid, *J. Phys. Chem. C*, 2010, **114**(6), 2421–2427, DOI: **10.1021/jp906960g**.

54 F. Waag, R. Streubel, B. Gökce and S. Barcikowski, Synthesis of gold, platinum, and gold-platinum alloy nanoparticle colloids with high-power megahertz-repetition-rate lasers: the importance of the beam guidance method, *Appl. Nanosci.*, 2021, **11**(4), 1303–1312, DOI: **10.1007/s13204-021-01693-y**.

55 B. Barcikowski, S. Amendola, V. Lau, M. Marzun, G. Rehbock, C. Reichenberger, S. Zhang and D. Gökce, *Handbook of Laser Synthesis & Processing of Colloids*, Duisburg-Essen Publication Online, Second edn, 2019.

56 N. L. Lahaye, S. S. Harilal, P. K. Diwakar and A. Hassanein, The effect of laser pulse duration on ICP-MS signal intensity, elemental fractionation, and detection limits in fs-LA-ICP-MS, *J. Anal. At. Spectrom.*, 2013, **28**(11), 1781–1787, DOI: **10.1039/c3ja50200g**.

57 K. Chaudhary, S. Z. H. Rizvi and J. Ali, Laser-Induced Plasma and its Applications, *Plasma Science and Technology - Progress in Physical States and Chemical Reactions*, InTech, 2016.

58 C. Y. Shih, R. Streubel, J. Heberle, A. Letzel, M. V. Shugaev, C. Wu, M. Schmidt, B. Gökce, S. Barcikowski and L. V. Zhigilei, Two mechanisms of nanoparticle generation in picosecond laser ablation in liquids: the origin of the bimodal size distribution, *Nanoscale*, 2018, **10**(15), 6900–6910, DOI: **10.1039/c7nr08614h**.

59 X. Li and Y. Guan, Theoretical fundamentals of short pulse laser-metal interaction: a review, *Nami Jishu Yu Jingmi Gongcheng*, 2020, **3**(3), 105–125, DOI: **10.1016/j.npe.2020.08.001**.

60 M. Dell'Aglio, R. Gaudiuso, O. De Pascale and A. De Giacomo, Mechanisms and processes of pulsed laser ablation in liquids during nanoparticle production, *Appl. Surf. Sci.*, 2015, **348**, 4–9, DOI: **10.1016/j.apsusc.2015.01.082**.

61 A. Kanitz, M. R. Kalus, E. L. Gurevich, A. Ostendorf, S. Barcikowski and D. Amans, Review on experimental and theoretical investigations of the early stage, femtoseconds to microseconds processes during laser ablation in liquid-phase for the synthesis of colloidal nanoparticles, *Plasma Sources Sci. Technol.*, 2019, **28**(10), 103001, DOI: **10.1088/1361-6595/ab3dbe**.

62 J. Long, M. Eliceiri, Z. Vangelatos, Y. Rho, L. Wang, Z. Shu, X. Xie, Y. Zhang and C. P. Grigoropoulos, Early dynamics of cavitation bubbles generated during ns laser ablation of submerged targets, *Opt. Express*, 2020, **28**(10), 14300, DOI: **10.1364/oe.391584**.

63 C.-Y. Shih, C. Wu, M. V. Shugaev and L. V. Zhigilei, Atomistic modeling of nanoparticle generation in short pulse laser ablation of thin metal films in water, *J. Colloid Interface Sci.*, 2017, **489**, 3–17, DOI: **10.1016/j.jcis.2016.10.029**.

64 S. Jendrzej, B. Gökce, V. Amendola and S. Barcikowski, Barrierless growth of precursor-free, ultrafast laser-fragmented noble metal nanoparticles by colloidal atom clusters – A kinetic in situ study, *J. Colloid Interface Sci.*, 2016, **463**, 299–307, DOI: **10.1016/j.jcis.2015.10.032**.

65 S. Ibrahimkutty, P. Wagener, T. D. S. Rolo, D. Karpov, A. Menzel, T. Baumbach, S. Barcikowski and A. Plech, A hierarchical view on material formation during pulsed-laser synthesis of nanoparticles in liquid, *Sci. Rep.*, 2015, **5**(1), 16313, DOI: **10.1038/srep16313**.

66 A. Hamad, L. Li and Z. Liu, A comparison of the characteristics of nanosecond, picosecond and femtosecond lasers generated Ag, TiO_2 and Au nanoparticles in deionised water, *Appl. Phys. A: Mater. Sci. Process.*, 2015, **120**(4), 1247–1260, DOI: **10.1007/s00339-015-9326-6**.

67 V. Amendola, D. Amans, Y. Ishikawa, N. Koshizaki, S. Scirè, G. Compagnini, S. Reichenberger and S. Barcikowski, Room-Temperature Laser Synthesis in Liquid of Oxide, Metal-Oxide Core–Shells, and Doped Oxide Nanoparticles, *Chem. – Eur. J.*, 2020, **26**(42), 9206–9242, DOI: **10.1002/chem.202000686**.

68 C. Y. Shih, M. V. Shugaev, C. Wu and L. V. Zhigilei, The effect of pulse duration on nanoparticle generation in pulsed laser ablation in liquids: insights from large-scale atomistic simulations, *Phys. Chem. Chem. Phys.*, 2020, **22**(13), 7077–7099, DOI: **10.1039/d0cp00608d**.

69 S. Shankar Naik, J. Theerthagiri, F. S. Nogueira, S. J. Lee, A. Min, G. A. Kim, G. Maia, L. M. C. Pinto and M. Y. Choi, Dual-Cation-Coordinated CoFe-Layered Double-Hydroxide Nanosheets Using the Pulsed Laser Ablation Technique for Efficient Electrochemical Water Splitting: Mechanistic Screening by In Situ/Operando Raman and Density Functional Theory Calculations, *ACS Catal.*, 2023, **13**(2), 1477–1491, DOI: **10.1021/acscatal.2c05017**.

70 R. C. Forsythe, C. P. Cox, M. K. Wilsey and A. M. Müller, Pulsed Laser in Liquids Made Nanomaterials for Catalysis, *Chem. Rev.*, 2021, **121**(13), 7568–7637, DOI: **10.1021/acs.chemrev.0c01069**.

71 S. A. Yehia, L.G. Carpen, F. Stokker-Cheregi, C. Poronicu, V. Sătulu, C. Staicu, B. Butoi, I. Lungu, F. Virot, C. Grisolia and G. Dinescu, Laser ablation of a solid target in liquid medium for beryllium nanoparticles synthesis, *Nucl. Mater. Energy*, 2022, **31**, 101160, DOI: 10.1016/j.nme.2022.101160.

72 S. N. Sanders, T. H. Schloemer, M. K. Gangishetty, D. Anderson, M. Seitz, A. O. Gallegos, R. C. Stokes and D. N. Congreve, Triplet fusion upconversion nanocapsules for volumetric 3D printing, *Nature*, 2022, **604**(7906), 474–478, DOI: 10.1038/s41586-022-04485-8.

73 H. Zeng, X. -W. Du, S. C. Singh, S. A. Kulinich, S. Yang, J. He and W. Cai, Nanomaterials via laser ablation/irradiation in liquid: a review, *Adv. Funct. Mater.*, 2012, **22**(7), 1333–1353, DOI: 10.1002/adfm.201102295.

74 R. Streubel, S. Barcikowski and B. Gökce, Continuous multigram nanoparticle synthesis by high-power, high-repetition-rate ultrafast laser ablation in liquids, *Opt. Lett.*, 2016, **41**(7), 1486, DOI: 10.1364/OL.41.001486.

75 F. Waag, B. Gökce and S. Barcikowski, Ablation target cooling by maximizing the nanoparticle productivity in laser synthesis of colloids, *Appl. Surf. Sci.*, 2019, **466**, 647–656, DOI: 10.1016/j.apsusc.2018.10.030.

76 S. Dittrich, S. Barcikowski and B. Gökce, Plasma and nanoparticle shielding during pulsed laser ablation in liquids cause ablation efficiency decrease, *Opto-Electron. Adv.*, 2021, **4**(1), 1–13, DOI: 10.29026/oea.2021.200072.

77 W. Haiss, N. T. K. Thanh, J. Aveyard and D. G. Fernig, Determination of Size and Concentration of Gold Nanoparticles from UV-Vis Spectra, *Anal. Chem.*, 2007, **79**(11), 4215–4221, DOI: 10.1021/ac0702084.

78 T. Hendel, M. Wuithschick, F. Kettemann, A. Birnbaum, K. Rademann and J. Polte, In situ determination of colloidal gold concentrations with UV-vis spectroscopy: limitations and perspectives, *Anal. Chem.*, 2014, **86**(22), 11115–11124, DOI: 10.1021/ac502053s.

79 J. Katyal and R. K. Soni, Size- and shape-dependent plasmonic properties of aluminum nanoparticles for nanosensing applications, *J. Mod. Opt.*, 2013, **60**(20), 1717–1728, DOI: 10.1080/09500340.2013.856483.

80 X. Liu, M. Atwater, J. Wang and Q. Huo, Extinction coefficient of gold nanoparticles with different sizes and different capping ligands, *Colloids Surf., B*, 2007, **58**(1), 3–7, DOI: 10.1016/j.colsurfb.2006.08.005.

81 S. P. Yeap, J. K. Lim, B. S. Ooi and A. L. Ahmad, Agglomeration, colloidal stability, and magnetic separation of magnetic nanoparticles: collective influences on environmental engineering applications, *J. Nanopart. Res.*, 2017, **19**(11), 368, DOI: 10.1007/s11051-017-4065-6.

82 P. L. Golas, S. Louie, G. V. Lowry, K. Matyjaszewski and R. D. Tilton, Comparative Study of Polymeric Stabilizers for Magnetite Nanoparticles Using ATRP, *Langmuir*, 2010, **26**(22), 16890–16900, DOI: 10.1021/la103098q.

83 T. Phenrat, N. Saleh, K. Sirk, R. D. Tilton and G. V. Lowry, Aggregation and Sedimentation of Aqueous Nanoscale Zerovalent Iron Dispersions, *Environ. Sci. Technol.*, 2007, **41**(1), 284–290, DOI: 10.1021/es061349a.

84 S. Reich, Patrick Schönfeld, P. Wagener, A. Letzel, S. Ibrahimkutty, B. Gökce, S. Barcikowski, A. Menzel, T. D. S. Rolo and A. Plech, Pulsed laser ablation in liquids: impact of the bubble dynamics on particle formation, *J. Colloid Interface Sci.*, 2017, **489**, 106–113, DOI: 10.1016/j.jcis.2016.08.030.

85 S. Dittrich, R. Streubel, C. McDonnell, H. P. Huber, S. Barcikowski and B. Gökce, Comparison of the productivity and ablation efficiency of different laser classes for laser ablation of gold in water and air, *Appl. Phys. A: Mater. Sci. Process.*, 2019, **125**(6), 1–10, DOI: 10.1007/s00339-019-2704-8.

86 M. R. Kalus, R. Lanyumba, N. Lorenzo-Parodi, M. A. Jochmann, K. Kerpen, U. Hagemann, T. C. Schmidt, S. Barcikowski and B. Gökce, Determining the role of redox-active materials during laser-induced water decomposition, *Phys. Chem. Chem. Phys.*, 2019, **21**(34), 18636–18651, DOI: 10.1039/c9cp02663k.

87 A. Resano-Garcia, S. Champmartin, Y. Battie, A. Koch, A. En Naciri, A. Ambari and N. Chaoui, Highly-repeatable generation of very small nanoparticles by pulsed-laser ablation in liquids of a high-speed rotating target, *Phys. Chem. Chem. Phys.*, 2016, **18**(48), 32868–32875, DOI: 10.1039/c6cp06511b.

88 S. Kohsakowski, A. Santagata, A. Dell'Aglio, A. de Giacomo, S. Barcikowski, P. Wagener and B. Gökce, High productive and continuous nanoparticle fabrication by laser ablation of a wire-target in a liquid jet, *Appl. Surf. Sci.*, 2017, **403**, 487–499, DOI: 10.1016/j.apsusc.2017.01.077.

89 G. C. Messina, P. Wagener, R. Streubel, A. De Giacomo, A. Santagata, G. Compagnini and S. Barcikowski, Pulsed laser ablation of a continuously-fed wire in liquid flow for high-yield production of silver nanoparticles, *Phys. Chem. Chem. Phys.*, 2013, **15**(9), 3093–3098, DOI: 10.1039/c2cp42626a.

90 P. Wagener, A. Schwenke, B. N. Chichkov and S. Barcikowski, Pulsed laser ablation of zinc in tetrahydrofuran: bypassing the cavitation bubble, *J. Phys. Chem. C*, 2010, **114**(17), 7618–7625, DOI: 10.1021/jp911243a.

91 Y. Monsa, G. Gal, N. Lerner and I. Bar, A simple strategy for enhanced production of nanoparticles by laser ablation in liquids, *Nanotechnology*, 2020, **31**(23), 235601, DOI: 10.1088/1361-6528/ab78ac.

92 P. F. S. Pereira, A. C. A. de Paula e Silva, B. N. A. da Silva Pimentel, I. M. Pinatti, A. Z. Simões, C. E. Vergani, D. F. Barreto-Vieira, M. A. N. da Silva, M. D. Miranda, M. E. S. Monteiro, A. Tucci, C. Doñate-Buendía, G. Mínguez-Vega, J. Andrés and E. Longo, Inactivation of SARS-CoV-2 by a chitosan/α-Ag_2WO_4 composite generated by femtosecond laser irradiation, *Sci. Rep.*, 2022, **12**(1), 8118, DOI: 10.1038/s41598-022-11902-5.

93 J. G. Cuadra, S. Molina-Prados, G. Mínguez-Vega, Ana. C. Estrada, T. Trindade, C. Oliveira, M. P. Seabra, J. Labrincha, S. Porcar, R. Cadena, D. Fraga and J. B. Carda, Multifunctional Silver-Coated Transparent TiO_2 Thin Films for Photocatalytic and Antimicrobial Applications, *Appl. Surf. Sci.*, 2023, **617**, 156519, DOI: 10.1016/j.apsusc.2023.156519.

94 C. Doñate-Buendia, R. Torres-Mendieta, A. Pyatenko, E. Falomir, M. Fernández-Alonso and G. Mínguez-Vega, Fabrication by Laser Irradiation in a Continuous Flow Jet of Carbon Quantum Dots for Fluorescence Imaging, *ACS Omega*, 2018, **3**(3), 2735–2742, DOI: 10.1021/acsomega.7b02082.

95 T. Hupfeld, A. Wegner, M. Blanke, C. Doñate-Buendía, V. Sharov, S. Nieskens, M. Piechotta, M. Giese, S. Barcikowski and B. Gökce, Plasmonic Seasoning: Giving Color to Desktop Laser 3D Printed Polymers by Highly Dispersed Nanoparticles, *Adv. Opt. Mater.*, 2020, **8**(15), 2000473, DOI: 10.1002/adom.202000473.

96 K. Sugioka and Y. Cheng, Ultrafast lasers-reliable tools for advanced materials processing, *Light: Sci. Appl.*, 2014, **3**(390), 1–12, DOI: 10.1038/lsa.2014.30.

97 S. I. Kudryashov, A. A. Nastulyavichus, A. K. Ivanova, N. A. Smirnov, R. A. Khmelnitskiy, A. A. Rudenko, I. N. Saraeva, E. R. Tolordava, A. Yu. Kharin, I. N. Zavestovskaya, Y. M. Romanova, D. A. Zayarny and A. A. Ionin, High-throughput laser generation of Si-nanoparticle based surface coatings for antibacterial applications, *Appl. Surf. Sci.*, 2019, **470**, 825–831, DOI: 10.1016/j.apsusc.2018.11.201.

98 A. Menéndez-Manjón, P. Wagener and S. Barcikowski, Transfer-matrix method for efficient ablation by pulsed laser ablation and nanoparticle generation in liquids, *J. Phys. Chem. C*, 2011, **115**(12), 5108–5114, DOI: 10.1021/jp109370q.

99 C. Doñate-Buendía, M. Fernández-Alonso, J. Lancis and G. Mínguez-Vega, Overcoming the barrier of nanoparticle production by femtosecond laser ablation in liquids using simultaneous spatial and temporal focusing, *Photonics Res.*, 2019, **7**(11), 1249, DOI: 10.1364/PRJ.7.001249.

100 S. Kohsakowski, B. Gökce, R. Tanabe, P. Wagener, A. Plech, Y. Ito and S. Barcikowski, Target geometry and rigidity determines laser-induced cavitation bubble transport and nanoparticle productivity-a high-speed videography study, *Phys. Chem. Chem. Phys.*, 2016, **18**(24), 16585–16593, DOI: 10.1039/c6cp01232a.

101 B. N. Chichkov, C. Momma, S. Nolte, F. Alvensleben and A. Tünnermann, Femtosecond, picosecond and nanosecond laser ablation of solids, *Appl. Phys. A: Mater. Sci. Process.*, 1996, **63**(2), 109–115, DOI: 10.1007/BF01567637.

102 S. Nolte, C. Momma, H. Jacobs, A. Tünnermann, B. N. Chichkov, B. Wellegehausen and H. Welling, Ablation of metals by ultrashort laser pulses, *J. Opt. Soc. Am. B*, 1997, **14**(10), 2716–2722, DOI: 10.1364/JOSAB.14.002716.

103 S. Preuss, A. Demchuk and M. Stuke, Sub-picosecond UV laser ablation of metals, *Appl. Phys. A: Mater. Sci. Process.*, 1995, **61**(1), 33–37, DOI: 10.1007/BF01538207.

104 G. Račiukaitis, M. Brikas, P. Gečys, B. Voisiat and M. Gedvilas, Use of high repetition rate and high power lasers in microfabrication: How to keep the efficiency high?, *J. Laser Micro Nanoeng.*, 2009, **4**(3), 186–191, DOI: 10.2961/jlmn.2009.03.0008.

105 B. Neuenschwander, B. Jaeggi, M. Schmid, V. Rouffiange and P.-E. Martin, Optimization of the volume ablation rate for metals at different laser pulse-durations from ps to fs, *Laser Appl. Microelectron. Optoelectron. Manuf. XVII*, 2012, **8243**, 824307, DOI: 10.1117/12.908583.

106 L. V. Zhigilei and B. J. Garrison, Microscopic mechanisms of laser ablation of organic solids in the thermal and stress confinement irradiation regimes, *J. Appl. Phys.*, 2000, **88**(3), 1281–1298, DOI: 10.1063/1.373816.

107 B. Le Drogoff, F. Vidal, S. Laville, M. Chaker, T. Johnston, O. Barthélemy, J. Margot and M. Sabsabi, Laser-ablated volume and depth as a function of pulse duration in aluminum targets, *Appl. Opt.*, 2005, **44**(2), 278–281, DOI: 10.1364/AO.44.000278.

108 A. Ostendorf, G. Kamlage, U. Klug, F. Korte and B. N. Chichkov, Femtosecond versus picosecond laser ablation (Keynote Address), *Phot. Process. Microelectron. Photonics IV*, 2005, **5713**, 1, DOI: 10.1117/12.597975.

109 R. Le Harzic, D. Breitling, M. Weikert, S. Sommer, C. Föhl, S. Valette, C. Donnet, E. Audouard and F. Dausinger, Pulse width and energy influence on laser micromachining of metals in a range of 100 fs to 5 ps, *Appl. Surf. Sci.*, 2005, **249**(1–4), 322–331, DOI: 10.1016/j.apsusc.2004.12.027.

110 A. Nastulyavichus, S. Kudryashov, A. Ionin and S. Gonchukov, Optimization of nanoparticle yield for biomedical applications at femto-, pico- and nanosecond laser ablation of thin gold films in water, *Laser Phys. Lett.*, 2022, **19**(4), 045603, DOI: 10.1088/1612-202X/ac581a.

111 S. Kudryashov, A. Samokhvalov, A. Nastulyavichus, I. Saraeva, V. Mikhailovskii, A. Ionin and V. Veiko, Nanosecond-Laser Generation of Nanoparticles in Liquids: From Ablation through Bubble Dynamics to Nanoparticle Yield, *Materials*, 2019, **12**(4), 562, DOI: 10.3390/ma12040562.

112 A. Nastulyavichus, N. Smirnov and S. Kudryashov, Quantitative evaluation of LAL productivity of colloidal nanomaterials: Which laser pulse width is more productive, ergonomic, and economic?, *Chin. Phys. B*, 2022, **31**(7), 077803, DOI: 10.1088/1674-1056/ac5602.

113 N. A. Smirnov, S. I. Kudryashov, A. A. Rudenko, A. A. Nastulyavichus and A. A. Ionin, Ablation efficiency of gold at fs/ps laser treatment in water and air, *Laser Phys. Lett.*, 2022, **19**(2), 026001, DOI: 10.1088/1612-202X/ac46ab.

114 S. Barcikowski, A. Meńndez-Manjón, B. Chichkov, M. Brikas and G. Račiukaitis, Generation of nanoparticle colloids by picosecond and femtosecond laser ablations in liquid flow, *Appl. Phys. Lett.*, 2007, **91**(8), 083113, DOI: 10.1063/1.2773937.

115 S. Kohsakowski, *Hochskalierung der laserbasierten Nanopartikelsynthese für die heterogene Katalyse*, University of Duisburg Essen, 2018.

116 A. Ancona, S. Döring, C. Jauregui, F. Röser, J. Limpert, S. Nolte and A. Tünnermann, Femtosecond and picosecond laser drilling of metals at high repetition rates and average powers, *Opt. Lett.*, 2009, **34**(21), 3304–3306, DOI: 10.1364/OL.34.003304.

117 A. Tunnermann and S. Nolte, Femtosecond vs. Picosecond Laser Material Processing Challenges in ultrafast precision laser Micro-machining of Metals at high repetition rates, *Pulse*, 2010, **49**(1), 34–38.

118 M. E. Povarnitsyn, T. E. Itina, P. R. Levashov and K. V. Khishchenko, Mechanisms of nanoparticle formation by ultra-short laser ablation of metals in liquid environment, *Phys. Chem. Chem. Phys.*, 2013, **15**(9), 3108–3114, DOI: 10.1039/c2cp42650a.

119 T. E. Itina, On nanoparticle formation by laser ablation in liquids, *J. Phys. Chem. C*, 2011, **115**(12), 5044–5048, DOI: 10.1021/jp1090944.

120 I. N. Saraeva, S. I. Kudryashov, A. A. Rudenko, M. I. Zhilnikova, D. S. Ivanov, D. A. Zayarny, A. V. Simakin, A. A. Ionin and M. E. Garcia, Effect of fs/ps laser pulsewidth on ablation of metals and silicon in air and liquids, and on their nanoparticle yields, *Appl. Surf. Sci.*, 2019, **470**, 1018–1034, DOI: 10.1016/j.apsusc.2018.11.199.

121 C. Ma and W. Lin, Normal dispersion effects on the nonlinear focus, *J. Opt. Soc. Am. B*, 2016, **33**(6), 1055–1059, DOI: 10.1364/JOSAB.33.001055.

122 D. Riabinina, M. Chaker and J. Margot, Dependence of gold nanoparticle production on pulse duration by laser ablation in liquid media, *Nanotechnology*, 2012, **23**(13), 135603, DOI: 10.1088/0957-4484/23/13/135603.

123 N. A. Smirnov, S. I. Kudryashov, A. A. Rudenko, D. A. Zayarny and A. A. Ionin, Pulsewidth and ambient medium effects during ultrashort-pulse laser ablation of silicon in air and water, *Appl. Surf. Sci.*, 2021, **562**, 150243, DOI: 10.1016/j.apsusc.2021.150243.

124 I. Bunaziv, O. M. Akselsen, X. Ren, B. Nyhus, M. Eriksson and S. Gulbrandsen-Dahl, A review on laser-assisted joining of aluminium alloys to other metals, *Metals*, 2021, **11**(11), 1680, DOI: 10.3390/met11111680.

125 T. Nakano, *Multi-dimensional Additive Manufacturing*, 2021.

126 D.-I. J. Berkmanns and D.-I. M. Faerber, *Laser basics - LASERLINE Technical.*, 2008.

127 T. Tsuji, K. Iryo, Y. Nishimura and M. Tsuji, Preparation of metal colloids by a laser ablation technique in solution: influence of laser wavelength on the ablation efficiency (II), *J. Photochem. Photobiol., A*, 2001, **145**(3), 201–207, DOI: 10.1016/S1010-6030(01)00583-4.

128 T. Tsuji, K. Iryo, N. Watanabe and M. Tsuji, Preparation of silver nanoparticles by laser ablation in solution: influence of laser wavelength on particle size, *Appl. Surf. Sci.*, 2002, **202**(1–2), 80–85, DOI: 10.1016/S0169-4332(02)00936-4.

129 T. Tsuji, D. H. Thang, Y. Okazaki, M. Nakanishi, Y. Tsuboi and M. Tsuji, Preparation of silver nanoparticles by laser ablation in polyvinylpyrrolidone solutions, *Appl. Surf. Sci.*, 2008, **254**(16), 5224–5230, DOI: 10.1016/j.apsusc.2008.02.048.

130 F. Mafuné, J. Y. Kohno, Y. Takeda, T. Kondow and H. Sawabe, Formation of gold nanoparticles by laser ablation in aqueous solution of surfactant, *J. Phys. Chem. B*, 2001, **105**(22), 5114–5120, DOI: 10.1021/jp0037091.

131 R. Intartaglia, K. Bagga and F. Brandi, Study on the productivity of silicon nanoparticles by picosecond laser ablation in water: towards gram per hour yield, *Opt. Express*, 2014, **22**(3), 3117, DOI: 10.1364/OE.22.003117.

132 B. Kumar and R. K. Thareja, Laser ablated copper plasmas in liquid and gas ambient, *Phys. Plasmas*, 2013, **20**(5), 053503, DOI: 10.1063/1.4807041.

133 A. De Giacomo, M. Dell'Aglio, A. Santagata, R. Gaudiuso, O. De Pascale, P. Wagener, G. C. Messina, G. Compagnini and S. Barcikowski, Cavitation dynamics of laser ablation of bulk and wire-shaped metals in water during nanoparticles production, *Phys. Chem. Chem. Phys.*, 2013, **15**(9), 3083–3092, DOI: 10.1039/c2cp42649h.

134 B. Kumar and R. K. Thareja, Synthesis of nanoparticles in laser ablation of aluminum in liquid, *J. Appl. Phys.*, 2010, **108**(6), 064906, DOI: 10.1063/1.3486517.

135 K. Sasaki and N. Takada, Liquid-phase laser ablation, *Pure Appl. Chem.*, 2010, **82**(6), 1317–1327, DOI: 10.1351/PAC-CON-09-10-23.

136 A. De Giacomo, R. Gaudiuso, M. Dell'Aglio and A. Santagata, The role of continuum radiation in laser induced plasma spectroscopy, *Spectrochim. Acta, Part B*, 2010, **65**(5), 385–394, DOI: 10.1016/j.sab.2010.03.016.

137 H. Ushida, N. Takada and K. Sasaki, Diagnostics of liquid-phase laser ablation plasmas by spectroscopic methods, *J. Phys.: Conf. Ser.*, 2007, **59**(1), 563–566, DOI: 10.1088/1742-6596/59/1/120.

138 J. Hoffman, J. Chrzanowska, T. Moscicki, J. Radziejewska, L. Stobinski and Z. Szymanski, Plasma generated during underwater pulsed laser processing, *Appl. Surf. Sci.*, 2017, **417**, 130–135, DOI: 10.1016/j.apsusc.2017.01.185.

139 A. Vogel, N. Linz, S. Freidank and G. Paltauf, Femtosecond-laser-induced nanocavitation in water: implications for optical breakdown threshold and cell surgery, *Phys. Rev. Lett.*, 2008, **100**(3), 1–4, DOI: 10.1103/PhysRevLett.100.038102.

140 J. Lam, J. Lombard, C. Dujardin, G. Ledoux, S. Merabia and D. Amans, Dynamical study of bubble expansion following laser ablation in liquids, *Appl. Phys. Lett.*, 2016, **108**(7), 1–6, DOI: 10.1063/1.4942389.

141 R. Tanabe, T. T. P. Nguyen, T. Sugiura and Y. Ito, Bubble dynamics in metal nanoparticle formation by laser ablation in liquid studied through high-speed laser stroboscopic videography, *Appl. Surf. Sci.*, 2015, **351**, 327–331, DOI: 10.1016/j.apsusc.2015.05.030.

142 A. Letzel, M. Santoro, J. Frohleiks, A. R. Ziefuß, S. Reich, A. Plech, E. Fazio, F. Neri, S. Barcikowski and B. Gökce, How the re-irradiation of a single ablation spot affects cavitation bubble dynamics and nanoparticles properties in laser ablation in liquids, *Appl. Surf. Sci.*, 2019, **473**, 828–837, DOI: 10.1016/j.apsusc.2018.12.025.

143 J. Long, M. H. Eliceiri, L. Wang, Z. Vangelatos, Y. Ouyang, X. Xie, Y. Zhang and C. P. Grigoropoulos, Capturing the final stage of the collapse of cavitation bubbles generated during nanosecond laser ablation of submerged targets, *Opt. Laser Technol.*, 2021, **134**, 106647, DOI: 10.1016/j.optlastec.2020.106647.

144 T. T. P. Nguyen, R. Tanabe-Yamagishi and Y. Ito, Effects of liquid depth on the expansion and collapse of a hemispherical cavitation bubble induced in nanosecond pulsed laser ablation of a solid in liquid, *Opt. Lasers Eng.*, 2020, **126**, 105937, DOI: 10.1016/j.optlaseng.2019.105937.

145 M. R. Kalus, N. Bärsch, R. Streubel, E. Gökce, S. Barcikowski and B. Gökce, How persistent microbubbles

shield nanoparticle productivity in laser synthesis of colloids – Quantification of their volume, dwell dynamics, and gas composition, *Phys. Chem. Chem. Phys.*, 2017, **19**(10), 7112–7123, DOI: 10.1039/c6cp07011f.

146 M. Dell'Aglio, A. Santagata, G. Valenza, A. De Stradis and A. De Giacomo, Study of the Effect of Water Pressure on Plasma and Cavitation Bubble Induced by Pulsed Laser Ablation in Liquid of Silver and Missed Variations of Observable Nanoparticle Features, *ChemPhysChem*, 2017, **18**(9), 1165–1174, DOI: 10.1002/cphc.201601231.

147 C. Doñate-Buendia, M. Spellauge, E. Streubel, F. Riahi, S. Barcikowski, H. P. Huber and B. Gökce, Double-pulse laser ablation in liquids: nanoparticle bimodality reduction by sub-nanosecond interpulse delay optimization, *J. Phys. D: Appl. Phys.*, 2023, **56**(10), 104001, DOI: 10.1088/1361-6463/acbaaa.

148 D. Franz, T. Häfner, T. Kunz, G-L. Roth, S. Rung, C. Esen and R. Hellmann, Characterization of a hybrid scanning system comprising acousto-optical deflectors and galvanometer scanners, *Appl. Phys. B: Lasers Opt.*, 2022, **128**(3), 55, DOI: 10.1007/s00340-022-07782-2.

149 G. R. B. E. Römer and P. Bechtold, Electro-optic and acousto-optic laser beam scanners, *Phys. Proc.*, 2014, **56**(C), 29–39, DOI: 10.1016/j.phpro.2014.08.092.

150 R. De Loor, Polygon Scanner System for Ultra Short Pulsed Laser Micro-Machining Applications, *Phys. Proc.*, 2013, **41**, 544–551, DOI: 10.1016/j.phpro.2013.03.114.

151 P. Bechtold, R. Hohenstein and M. Schmidt, Evaluation of disparate laser beam deflection technologies by means of number and rate of resolvable spots, *Opt. Lett.*, 2013, **38**(16), 2934–2937, DOI: 10.1364/OL.38.002934.

152 Raylase, SUPERSCAN IV-15 2-Axis Deflection Units, www.raylase.com, 2020. https://www.raylase.de/_Resources/Persistent/9/5/d/a/95da1035b2c564183914aa6c26c6f6e43f20044c/RAYLASE_SUPERSCANIV-15_en.pdf (accessed Feb. 26, 2023).

153 J. Schille, L. Schneider, A. Streek, S. Kloetzer and U. Loeschner, High-throughput machining using high average power ultrashort pulse lasers and ultrafast polygon scanner, *Proc. SPIE*, 2016, **9736**, 97360R, DOI: 10.1117/12.2220112.

154 S. Kudryashov, P. Danilov, L. Schneider, J. Schille, U. Loeschner, A. Nastulyavichus, N. Smirnov, A. Kuchmizhak and O. Vitrik, Polygon-facilitated generation of colloidal gold nanoparticles by multi-MHz ultrashort-pulse laser trains: key optical factors, *Laser Phys. Lett.*, 2021, **18**(1), 016101, DOI: 10.1088/1612-202X/abd171.

155 M. R. Kalus, V. Reimer, S. Barcikowski and B. Gökce, Discrimination of effects leading to gas formation during pulsed laser ablation in liquids, *Appl. Surf. Sci.*, 2019, **465**, 1096–1102, DOI: 10.1016/j.apsusc.2018.09.224.

156 M. R. Kalus, R. Lanyumba, S. Barcikowski and B. Gökce, Discrimination of ablation, shielding, and interface layer effects on the steady-state formation of persistent bubbles under liquid flow conditions during laser synthesis of colloids, *J. Flow Chem.*, 2021, **11**, 773–792, DOI: 10.1007/s41981-021-00144-7.

157 R. Lahoz, A. Naghilou, W. Kautek and O. Bomati-Miguel, Study of the physicochemical surface alterations and incubation phenomena induced on iron targets by nanosecond pulsed laser ablation in liquids: effect on productivity and characteristics of the synthesized nanoscale zero-valent iron (nZVI) particles, *Appl. Surf. Sci.*, 2020, **511**, 145438, DOI: 10.1016/j.apsusc.2020.145438.

158 R. Nadarajah, S. Barcikowski and B. Gökce, Picosecond laser-induced surface structures on alloys in liquids and their influence on nanoparticle productivity during laser ablation, *Opt. Express*, 2020, **28**(3), 2909, DOI: 10.1364/oe.28.002909.

159 W. Charee, V. Tangwarodomnukun and C. Dumkum, Laser ablation of silicon in water under different flow rates, *Int. J. Adv. Des. Manuf. Technol.*, 2015, **78**(1–4), 19–29, DOI: 10.1007/s00170-014-6625-6.

160 P. Nandini, K. Akash, G. Rohit, S. Vipul and I. A. Palani, Investigations on the Influence of Liquid-Assisted Laser Ablation of NiTi Rotating Target to Improve the Formation Efficiency of Spherical Alloyed NiTi Nanoparticles, *J. Mater. Eng. Perform.*, 2017, **26**(10), 4707–4717, DOI: 10.1007/s11665-017-2886-1.

161 G. Marzun, A. Levish, V. Mackert, T. Kallio, S. Barcikowski and P. Wagener, Laser synthesis, structure and chemical properties of colloidal nickel-molybdenum nanoparticles for the substitution of noble metals in heterogeneous catalysis, *J. Colloid Interface Sci.*, 2017, **489**, 57–67, DOI: 10.1016/j.jcis.2016.09.014.

162 Y. Jiang, P. Liu, Y. Liang, H. B. Li and G. W. Yang, Promoting the yield of nanoparticles from laser ablation in liquid, *Appl. Phys. A: Mater. Sci. Process.*, 2011, **105**(4), 903–907, DOI: 10.1007/s00339-011-6557-z.

163 V. Piotto, L. Litti and M. Meneghetti, Synthesis and Shape Manipulation of Anisotropic Gold Nanoparticles by Laser Ablation in Solution, *J. Phys. Chem. C*, 2020, **124**(8), 4820–4826, DOI: 10.1021/acs.jpcc.9b10793.

164 A. Syafiuddin, S. Salmiati, M. R. Salim, A. Beng Hong Kueh, T. Hadibarata and H. Nur, A Review of Silver Nanoparticles: Research Trends, Global Consumption, Synthesis, Properties, and Future Challenges, *J. Chin. Chem. Soc.*, 2017, **64**(7), 732–756, DOI: 10.1002/jccs.201700067.

165 S. F. Wirtz, A. P. A. Cunha, M. Labusch, G. Marzun, S. Barcikowski and D. Söffker, Development of a low-cost FPGA-based measurement system for real-time processing of acoustic emission data: proof of concept using control of pulsed laser ablation in liquids, *Sensors*, 2018, **18**(6), 1–11, DOI: 10.3390/s18061775.

166 S. Crivellaro, A. Guadagnini, D. M. Arboleda, D. Schinca and V. Amendola, A system for the synthesis of nanoparticles by laser ablation in liquid that is remotely controlled with PC or smartphone, *Rev. Sci. Instrum.*, 2019, **90**(3), 033902, DOI: 10.1063/1.5083811.

167 M. Labusch, A. P. A. Cunha, S. F. Wirtz, S. Reichenberger, E. Cleve, D. Söffker and S. Barcikowski, Acoustic emission control avoids fluence shifts caused by target runaway during laser synthesis of colloids, *Appl. Surf. Sci.*, 2019, **479**, 887–895, DOI: 10.1016/j.apsusc.2019.02.080.

168 B. Freeland, R. McCann, G. Alkan, B. Friedrich, G. Foley and D. Brabazon, Stable nano-silver colloid production via Laser Ablation Synthesis in Solution (LASiS) under laminar recirculatory flow, *Adv. Mater. Process. Technol.*, 2020, **6**(4), 677–685, DOI: **10.1080/2374068X.2020.1740877**.

169 S. Zhu, Y. F. Lu, M. H. Hong and X. Y. Chen, Laser ablation of solid substrates in water and ambient air, *J. Appl. Phys.*, 2001, **89**(4), 2400–2403, DOI: **10.1063/1.1342200**.

170 F. Waag, Y. Li, A.R. Ziefuß, E. Bertin, M. Kamp, V. Duppel, G. Marzun, L. Kienle, S. Barcikowski and B. Gökce, Kinetically-controlled laser-synthesis of colloidal high-entropy alloy nanoparticles, *RSC Adv.*, 2019, **9**(32), 18547–18558, DOI: **10.1039/c9ra03254a**.

171 C. Han, R. Wang, A. Pan, W. Wang, H. Huang, J. Zhang and C. Niu, Morphology-directing transformation of carbon nanotubes under the irradiation of pulsed laser with different pulsed duration, *Opt. Laser Technol.*, 2019, **109**, 27–32, DOI: **10.1016/j.optlastec.2018.07.058**.

172 M. Nazemi, S. R. Panikkanvalappil, C. K. Liao, M. A. Mahmoud and M. A. El-Sayed, Role of Femtosecond Pulsed Laser-Induced Atomic Redistribution in Bimetallic Au-Pd Nanorods on Optoelectronic and Catalytic Properties, *ACS Nano*, 2021, **15**(6), 10241–10252, DOI: **10.1021/acsnano.1c02347**.

173 K. Zhang, D. S. Ivanov, R. A. Ganeev, G. S. Boltaev, P. S. Krishnendu, S. C. Singh, M. E. Garcia, I. N. Zavestovskaya and C. Guo, Pulse duration and wavelength effects of laser ablation on the oxidation, hydrolysis, and aging of aluminum nanoparticles in water, *Nanomaterials*, 2019, **9**(5), 767, DOI: **10.3390/nano9050767**.

174 G. González-Rubio, P. Díaz-Núñez, A. Rivera, A. Prada, G. Tardajos, J. González-Izquierdo, L. Bañares, P. Llombart, L. G. Macdowel, M. A. Palafox, L. M. Liz-Marzán, O. Peña-Rodríguez and A. Guerrero-Martínez, Femtosecond laser reshaping yields gold nanorods with ultranarrow surface plasmon resonances, *Science*, 2017, **358**(6363), 640–644, DOI: **10.1126/science.aan8478**.

175 M. Curcio, A. De Bonis, A. Santagata, A. Galasso and R. Teghil, Effect of laser pulse duration on properties of metal and metal carbide nanoparticles obtained by laser in liquid synthesis, *Opt. Laser Technol.*, 2021, **138**, 106916, DOI: **10.1016/j.optlastec.2021.106916**.

176 J. Xiao, G. Ouyang, P. Liu, C. X. Wang and G. W. Yang, Reversible nanodiamond-carbon onion phase transformations, *Nano Lett.*, 2014, **14**(6), 3645–3652, DOI: **10.1021/nl5014234**.

177 Z. Wang, B. Xiao, Z. Lin, S. Shen, A. Xu, Z. Du, Y. Chen and W. Zhong, In situ surface decoration of RuO_2 nanoparticles by laser ablation for improved oxygen evolution reaction activity in both acid and alkali solutions, *J. Energy Chem.*, 2021, **54**, 510–518, DOI: **10.1016/j.jechem.2020.06.042**.

178 G. K. Yogesh, S. Shukla, D. Sastikumar and P. Koinkar, Progress in pulsed laser ablation in liquid (PLAL) technique for the synthesis of carbon nanomaterials: a review, *Appl. Phys. A: Mater. Sci. Process.*, 2021, **127**(11), 810, DOI: **10.1007/s00339-021-04951-6**.

179 M. Dell'Aglio, V. Motto-Ros, F. Pelascini, I. B. Gornushkin and A. De Giacomo, Investigation on the material in the plasma phase by high temporally and spectrally resolved emission imaging during pulsed laser ablation in liquid (PLAL) for NPs production and consequent considerations on NPs formation, *Plasma Sources Sci. Technol.*, 2019, **28**(8), 085017, DOI: **10.1088/1361-6595/ab369b**.

180 J. Johny, M. Kamp, O. Prymak, A. Tymoczko, U. Wiedwald, C. Rechbock, U. Schürmann, R. Popescu, D. Gerthsen, L. Kienle, S. Shaji and S. Barcikowski, Formation of Co–Au Core–shell nanoparticles with thin gold shells and soft magnetic ε-cobalt cores ruled by thermodynamics and kinetics, *J. Phys. Chem. C*, 2021, **125**(17), 9534–9549, DOI: **10.1021/acs.jpcc.1c02138**.

181 D. Spadaro, M. A. Iatì, M. G. Donato, P. G. Gucciardi, R. Saija, A. R. Cherlakola, S. Scaramuzza, V. Amendola and O. M. Maragò, Scaling of optical forces on Au–PEG core–shell nanoparticles, *RSC Adv.*, 2015, **5**(113), 93139–93146, DOI: **10.1039/c5ra20922f**.

182 X. Li, G. Zhang, L. Jiang, Z. Shi, K. Zhang, W. Rong, J. Duan and Y. Lu, Production rate enhancement of size-tunable silicon nanoparticles by temporally shaping femtosecond laser pulses in ethanol, *Opt. Express*, 2015, **23**(4), 4226–4232, DOI: **10.1364/OE.23.004226**.

183 M. Dell'Aglio, R. Gaudiuso, R. Elrashedy, O. De Pascale, G. Palazzo and A. De Giacomo, Collinear double pulse laser ablation in water for the production of silver nanoparticles, *Phys. Chem. Chem. Phys.*, 2013, **15**(48), 20868–20875, DOI: **10.1039/c3cp54194k**.

184 B. Liu, Z. Hu and Y. Che, *Nanoparticle production in liquid with multiple-pulse ultrafast laser ablation*, US 2011/0192714 A1, 2011.

185 G. Mínguez-Vega, J. Lancis, J. Caraquitena, V. Torres-Company and P. Andrés, High spatiotemporal resolution in multifocal processing with femtosecond laser pulses, *Opt. Lett.*, 2006, **31**(17), 2631–2633, DOI: **10.1364/ol.31.002631**.

186 O. Mendoza-Yero, G. Mínguez-Vega and J. Lancis, Encoding complex fields by using a phase-only optical element, *Opt. Lett.*, 2014, **39**(7), 1740, DOI: **10.1364/ol.39.001740**.

187 J. Cao, Q. Yang, Y. Miao, Y. Li, S. Qiu, Z. Zhu, P. Wang and Z. Chen, Enhance the delivery of light energy ultra-deep into turbid medium by controlling multiple scattering photons to travel in open channels, *Light: Sci. Appl.*, 2022, **11**(1), 108, DOI: **10.1038/s41377-022-00795-8**.

